Divergent Outcomes Of Myeloid Cell Infection By Gammaherpesvirus 68 Reveal Stepwise Regulation By Host And Viral Factors

Gabrielle Vragel[1], Kyra S. Noell[1,2], Ashley Tseng[1,2], Rachael E. Kostelecky[1], Elizabeth A. Alexander[1], Shirli Cohen[1], Catalina Galvan[1], Manaal Dalwadi[1], Brittany D. Gomez[1], Eva M. Medina[3], Darby G. Oldenburg[4], Andrew Goodspeed[5,6], Eric T. Clambey[2]*, Linda F. van Dyk[1]*#

Affiliations:

[1] Department of Immunology and Microbiology, [2] Department of Anesthesiology, [3] Department of Biochemistry and Molecular Genetics, University of Colorado Denver | Anschutz Medical Campus, School of Medicine, Aurora, CO, 80045, USA

[4] Gundersen Medical Foundation, Emplify Health System, La Crosse, Wisconsin, USA

[5] Department of Biomedical Informatics, [6] University of Colorado Cancer Center, University of Colorado Denver | Anschutz Medical Campus, School of Medicine, Aurora, CO, 80045, USA

*** Co-Corresponding authors:**

Eric T. Clambey, eric.clambey@cuanschutz.edu, 303-724-7783 (phone)

Linda F. van Dyk, linda.vandyk@cuanschutz.edu, 303-724-4207 (phone)

 # Lead author for MS correspondence

Linda F. van Dyk, linda.vandyk@cuanschutz.edu, 303-724-4207 (phone)

ORCIDs

https://orcid.org/0000-0001-9167-3013 (G.V.); 0000-0003-3623-8822 (K.S.N.); 0000-0002-3078-3718 (A.T.); 0000-0002-6529-3831 (R.E.K.); 0000-0002-4859-4122 (E.A.A.); 0000-0002-0253-786X (S.C.); 0009-0009-3439-7644 (C.G.); 0009-0005-3187-7803 (M.K.D); 0000-0002-3871-3773 (B.D.G.); 0000-0001-6899-0213 (E.M.M.); 0000-0003-2090-7489 (D.O.); 0000-0001-7055-7128 (A.G.); 0000-0002-7972-9544 (E.T.C.); 0000-0003-2662-5554 (L.F.v.D.)

Summary

The gammaherpesviruses establish a lifelong infection, with the cellular outcome of infection intimately regulated by cell type. Though myeloid cells are an early infection target, infection results in widely divergent outcomes without a clear explanation. Here we use murine gammaherpesvirus 68 to demonstrate that macrophages are readily infectable, resulting in three divergent infection outcomes dictated by viral and host factors. Infection in vivo and in a cell culture model results in a high frequency of viable cells characterized by restricted viral transcription and unexpected transcription of the ORF75 locus, with rare cells initiating but failing to complete lytic replication. In contrast, infection with a high viral dose triggers abortive infection and cell death. Restricted infection can be fully converted to productive lytic replication by pre-treatment with the host cytokine IL-4. These studies demonstrate stepwise regulation of virus infection and identify virus and host factors that dictate divergent outcomes in a single cell type.

42 **Introduction**

43 The gammaherpesviruses (γHVs), including the human viruses Epstein-Barr Virus (EBV) and
44 Kaposi's sarcoma-associated herpesvirus (KSHV or HHV-8), are large double-stranded DNA
45 tumor viruses. The γHVs establish a lifelong infection and are associated with chronic
46 inflammation and cancer, particularly in immunosuppressed individuals [1-3]. Due to the strict
47 host specificity of the human γHVs, murine gammaherpesvirus 68 (MHV68, γHV68 or MuHV-4)
48 has been extensively used as a genetic and phenotypically relevant model to study γHV
49 infection and pathogenesis in vivo [4, 5]. The γHVs infect multiple cell types, resulting in a range
50 of outcomes including lytic infection characterized by active virus replication or quiescent latent
51 infection [1], dictated by target cell type-specific virus-host interactions. Infection outcomes at
52 the single-cell level can be heterogeneous, including abortive infection [6-10].

53

54 Myeloid cells, including macrophages, monocytes and dendritic cells are innate immune cells
55 that have critical functions during γHV infection: they promote the early antiviral response yet
56 are also targeted for infection and subject to viral manipulation. While there is clear evidence
57 that KSHV, EBV and MHV68 infect myeloid cells [11-23], the state of infection in these cells
58 remains ambiguous, with evidence for both lytic transcription [19, 24, 25] and latent infection
59 [15, 18]; infection also appears to be abortive or unstable over time [26]. In some cases, myeloid
60 cells are thought to facilitate transit to B cells where γHVs establish long-term latent infection
61 [14, 26, 27]. γHV infection has also been shown to alter myeloid cell function, including KSHV-
62 induced differentiation of dysfunctional macrophages [22], manipulation of innate immune
63 signaling [16, 28, 29], and impaired function [30].

64

65 The most detailed insights regarding macrophage infection in vivo have come from the MHV68
66 system. MHV68 lytically replicates in macrophages prior to B cell infection [14, 27, 31]; MHV68

67 also establishes long-term latent infection in macrophages [15, 32]. While MHV68 passage
68 through alveolar macrophages and marginal zone macrophages promotes establishment of B
69 cell latency [14, 33], subcapsular sinus macrophages limit [34]. Macrophage infection is further
70 regulated by viral (ORF4, ORF36 [24, 25]) and host factors (e.g. interleukin (IL)-4 and IL-13,
71 Liver X receptors, cholesterol synthesis, type I and II interferons [35-38]).
72
73 Here, we sought to define γHV macrophage infection outcomes with a new level resolution
74 using the MHV68 system. Early macrophage infection in vivo is dominated by cells with frequent
75 transcription of the ORF75 locus, a γHV-conserved gene expressed in Kaposi's sarcoma lesions
76 and in EBV-transformed latently-infected B cells [39-42]. Using a reductionist system, we find
77 that MHV68 robustly infects macrophages with three distinct outcomes regulated by virus and
78 host factors: i) a restricted form of infection with rare cells undergoing lytic replication, ii) a
79 transcriptionally distinct form of abortive replication accompanied by high rates of cell death, and
80 iii) fully productive lytic replication. These studies emphasize that macrophage infection is
81 subject to multiple levels of control, resulting in diverse infection outcomes in a single cell type.

82 **RESULTS**

83 **Single cell RNA sequencing analysis of acute MHV68 macrophage infection reveals two**
84 **distinct transcriptional profiles.**

85 MHV68 macrophage infection has been associated with both lytic replication and latent
86 infection [14, 15, 24, 32], potentially serving as an important intermediary prior to B-cell latency
87 [14]. Despite these insights, the exact nature of myeloid cell infection remains incompletely
88 characterized. To define the viral transcriptional signatures at the earliest stages of macrophage
89 infection in vivo, we sort-purified MHV68 infected peritoneal macrophages from
90 immunocompetent C57BL/6J mice at 16 hours post-infection, followed by single-cell RNA-
91 sequencing (scRNA-seq). MHV68 infected cells were purified based on expression of a viral
92 reporter gene encoded by the latency-associated nuclear antigen fused with the beta-lactamase
93 enzyme (LANAβlac), a sensitive system that enables the direct identification and purification of
94 both lytic- and latently-infected cells [43, 44]. As expected, Seurat-based clustering and UMAP-
95 based visualization identified a dominant cluster of LANA+ peritoneal macrophages, with minor
96 cell subsets including: i) macrophages with a proliferative gene signature (i.e. "macrophage
97 proliferating"), ii) macrophages with an MHV68 lytic gene signature (i.e. "macrophage lytic"),
98 defined by expression of two canonical lytic genes ORF7 and ORF54, and infrequent iii) B cells,
99 iv) monocytes, v) dendritic cells and vi) T cells (Fig. 1A-C, Fig. S1A). Quality control metrics
100 were relatively comparable across all cell subsets, including the "macrophage lytic" subset (Fig.
101 S1B-E).

102 When we visualized and quantified the frequency of cells with detectable viral unique
103 molecular identifiers (UMIs), the majority (n=7,512; 82.54%) of LANA+ macrophages had
104 detectable viral reads accounting for <0.1% of total UMIs per cell (Fig. 1D-E). In contrast rare
105 macrophages with a lytic signature were characterized by a higher proportion (>0.1%) of viral
106 reads per cell (Fig. 1D-E). The presence of cells with no detectable viral UMIs could either be
107 due to the depth of sequencing or to the known sparseness of scRNA-seq data [45]. Increased

108 granularity of cell clustering identified 14 cell clusters (Fig. S2) but did not significantly change
109 defined cell populations nor the percentage of viral UMIs detected per cell subsets defined in
110 Figure 1.

111 Next, we quantified the frequency of macrophages that expressed each viral gene,
112 comparing the dominant macrophage population (n=9101 cells), with rare macrophages
113 characterized by a proliferative (n=48 cells) or lytic (n=25 cells) gene expression signature. We
114 detected ORF73-βlac mRNA, the transcript encoding the LANAβlac reporter by which cells were
115 purified, in 12.89% of macrophages, with equivalent or higher frequencies of detection for only 3
116 other viral genes: ORF75C (30.75%), ORF75B (27.83%) and ORF75A (12.54%) (Fig. 2A).
117 Additional transcripts were detected in a lower frequency of cells: ORF72 (5.3%), ORF58
118 (3.5%), with detectable RNA for M3, ORF7, ORF50, ORF57, ORF61, ORF74, M12, M13, or
119 M14 in 1-3% of cells (yellow circles, Fig. 2A). Remaining viral genes were only sporadically
120 detected (<1% of cells). A similar hierarchy, albeit reduced in magnitude, was observed in
121 proliferative macrophages (Fig. 2B). In contrast, rare lytic macrophages had a distinct viral gene
122 signature: multiple lytic cycle-associated genes (ORF7, ORF54, ORF57, ORF58, and ORF61)
123 were detected in 100% of cells (dark blue circles, Fig. 2C), with many more lytic cycle RNAs
124 (M3, ORF6, ORF21, ORF38, ORF50, ORF52, ORF59, ORF72 and ORF75C) detected in >75%
125 of cells (light blue circles, Fig. 2C). Detection of multiple, canonical lytic cycle RNAs in these
126 cells is consistent with these cells initiating lytic gene transcription in vivo.

127 The ORF75 locus is conserved among γHVs, with MHV68 containing triplicated ORF75
128 genes, ORF75A, ORF75B and ORF75C [4, 46]. Previous studies of this locus have revealed
129 multiple transcriptional units, including a polycistronic RNA that spans from the 5' end of
130 ORF75A through the 3' end of ORF75C [46]. Though these genes likely arose from gene
131 duplication, there is no significant similarity between the 3' ends of ORF75A and ORF75B or
132 ORF75A and ORF75C; only 22 of 26 nucleotides align between the final 150 nucleotides of
133 ORF75B and ORF75C (defined by blastn [47], data not shown). The nucleotide divergence

134 between ORF75 genes strongly suggests that UMIs mapping to each ORF75 gene were not
135 due to mapping errors. Notably, 50.89% of LANAβlac+ macrophages had detectable expression
136 of ORF75A, ORF75B and/or ORF75C (Fig. 2D). These studies identify two distinct
137 transcriptional signatures early after infection in vivo: 1) a high frequency of macrophages
138 expressing transcripts from the ORF75 locus, 2) with rare cells characterized by lytic
139 transcription.
140
141 **MHV68 readily infects J774 macrophages with limited lytic transcription.**
142 We next examined whether these viral outcomes could be observed in a reductionist cell
143 culture model, assessing MHV68 infection in the murine myeloid-like cell line, J774, compared
144 to 3T12 fibroblasts, a permissive murine fibroblast cell line [48]. As expected, MHV68 underwent
145 robust lytic replication in 3T12s with extensive cytopathic effect (CPE) by 72 hours post infection
146 (hpi). In contrast, MHV68-infected cultures of J774 cells showed minimal evidence of infection,
147 with no discernable CPE (Fig. 3A) and minimal viral genome replication or virus particle
148 production above input virus (Fig. 3B-C). Infection with WT MHV68.LANAβlac resulted in a
149 comparable frequency of LANAβlac+ cells in 3T12s fibroblasts and J774 cells (Fig. 3D-E, Fig.
150 S3A), demonstrating that J774 cells are fully susceptible to MHV68 infection, initiating
151 transcription and translation of ORF73 (an immediate early gene), with restricted infectious virus
152 particle production.
153 We next analyzed viral transcription in MHV68-infected J774 cells. ORF75A, ORF75B
154 and ORF75C were readily detected in MHV68-infected J774 cells, albeit at lower levels than
155 infected 3T12 cells (Fig. 3F, Fig. S3B). ORF75A expression was relatively comparable to
156 ORF73, with minimal change in expression between 24 and 48 hpi, suggesting constitutive
157 transcription of ORF73 and ORF75A (Fig. 3F). In contrast, ORF75B and ORF75C transcript
158 levels were moderately lower than ORF73 at 16 and 24 hpi, with ~4- and ~22 fold increase

159 between 24 and 48 hpi, respectively (right panel, Fig. 3F), potentially reflecting a subset of J774
160 cells initiating lytic infection. To assess lytic transcription, we quantified immediate early (IE)
161 (ORF73), early/late (ORF6), and late gene (M7) expression [49]. ORF73 (and Blac) expression
162 was reduced ~10 fold in J774 myeloid cells relative to 3T12 fibroblasts (Fig. 3G, Fig. S3C-D),
163 with ORF6 and M7 transcripts decreased >100 fold (Fig. 3G), consistent with greater deficits in
164 lytic gene expression at later stages of the lytic cycle in MHV68-infected J774 macrophages.
165 ORF6 and M7 expression increased ~10x between 24 hpi and 48 hpi (Fig. 3G, right panel),
166 consistent with some lytic transcription in MHV68-infected J774 cultures.
167
168 **Only rare MHV68 infected macrophages display lytic gene expression.**
169 We next defined the frequency of cells with lytic gene expression using a series of flow
170 cytometry-based assays. First, we infected 3T12 and J774 cells with a recombinant WT MHV68
171 virus, MHV68.HygroGFP (MHV68.H.GFP), that encodes a hygromycin resistance protein-GFP
172 fusion under the transcriptional control of the human cytomegalovirus IE promoter inserted
173 between ORF27 and 29b [50]. This virus robustly expresses GFP during active, lytic infection,
174 identifying cells that initiated lytic transcription and translation. 3T12 cells had a much higher
175 frequency of HygroGFP+ cells than J774 cells at 18 hpi (~8.2% vs. ~0.5% GFP+ respectively,
176 Fig. 4A-B, Fig. S3A); a similar low frequency of HygroGFP+ cells was observed in both J774
177 and RAW264.7 macrophage cell lines (Fig. S4A). Infection with two additional reporter viruses,
178 encoding either an ORF59GFP gene fusion [51] or a viral cyclin-beta lactamase gene fusion
179 (vCycβlac), further demonstrated that J774 cells had a greatly reduced frequency of reporter
180 gene positive events compared to 3T12 fibroblasts (Fig. 4C-D). The reduced frequency of lytic
181 gene expression in J774 cells was further observed when we analyzed two proteins associated
182 with lytic replication, the viral regulator of complement activation (vRCA), a protein encoded by
183 the ORF4 late gene, or phosphorylated histone H2AX (γH2AX), a host protein that undergoes
184 virus-induced phosphorylation [24]. Whereas ~45% of MHV68-infected 3T12 cells were

185 vRCA+, γH2AX+, or vRCA+γH2AX+ by 24 hpi, the frequency of MHV68-infected J774 cells that
186 expressed either of these proteins was significantly lower (~2% cells at 24 hpi, ~8% at 48 hpi)
187 (Fig. 4E-F, Fig. S4B). Given the low frequency of cells expressing lytic cycle genes, we tested
188 whether virally-infected J774 cells were capable of long-term growth and survival by purifying
189 LANAβlac+ J774 cells. Over 14 days, LANAβlac+ J774 cells showed a progressive growth
190 impairment relative to mock-infected cells, with limited evidence of viral replication (Fig. S4C-I).
191 These data indicate that MHV68-infected J774 cells rarely undergo lytic gene expression,
192 mirroring in vivo findings, and suggest the utility of this system to interrogate MHV68-myeloid
193 cell interactions.
194
195 **High dose MHV68 infection results in abortive replication.**
196 Our studies to this point focused on infection using an intermediate infectious dose, a
197 multiplicity of infection (MOI) of 1 plaque forming unit per cell. Since high MOI has been
198 implicated in overcoming intrinsic antiviral immunity [52, 53], we next compared infection
199 outcomes at an intermediate (MOI=1) or high inoculum (MOI=10). J774 cells infected with
200 intermediate MOI had a low frequency of HygroGFP+ cells (~4%); in contrast, infection with high
201 MOI was characterized by a dramatically increased frequency of HygroGFP+ cells (~92% cells)
202 (Fig. 5A-B). Similar increases in lytic gene expression were observed following high-dose
203 infection, quantifying: i) the frequency of ORF59GFP+ cells (Fig. 5C) and ii) the frequency of
204 cells characterized by actin RNA degradation (Fig. 5D), a hallmark of virus-induced host shutoff
205 that occurs during lytic replication [6, 54]. Despite these increased measures of lytic infection,
206 high-dose cultures were characterized by only modest increases in viral RNAs using bulk
207 cultures (Fig. 5E), with high rates of cell death (Fig. 5F), and minimal evidence of viral DNA
208 replication or infectious virus production over input (Fig. 5G-H). These data suggest that high-
209 dose infection of J774 cells results in an abortive lytic infection, characterized by increased early

210 signs of lytic gene expression, with a failure to complete viral DNA replication or infectious virus
211 production, potentially as a result of high rates of cell death.
212
213 **MHV68 infection of macrophages is modulated by viral and host factors.**
214 Given that interleukin (IL)-4 induces viral replication and reactivation from latency in
215 MHV68-infected primary macrophages [37, 55], we tested whether IL-4 pre-treatment was
216 sufficient to overcome the blocks on lytic replication following infection with an intermediate
217 dose. J774 cells pre-treated with IL-4 had a greatly enhanced frequency of HygroGFP+ cells
218 with ~60% GFP+ cells by 48 hpi (Fig. 6A-B), resulting in a time- and concentration-dependent
219 increase in viral DNA replication relative to untreated cells (Fig. 6C), culminating in increased
220 infectious virus production (Fig. 6D). These data demonstrate that IL-4 pre-treatment is
221 sufficient to overcome restricted MHV68 replication in macrophages and demonstrate that J774
222 cells are fully competent to support MHV68 lytic replication.
223 To begin to define how viral factors regulate macrophage infection, we examined two
224 viral genes: the viral cyclin (vCyc), dispensable for lytic replication in fibroblasts but critical for
225 reactivation from latency [56], and the immediate early transactivator Rta, which is essential for
226 lytic replication and capable of initiating reactivation from latency [57-59]. vCyc-deficient MHV68
227 infection was associated with a greatly reduced frequency of cells that expressed either vRCA
228 and/or γH2AX relative to WT MHV68-infected cells (Fig. 6E). Conversely, infection with a virus
229 that overexpresses Rta (CA-RTA MHV68) was associated with a greatly increased frequency of
230 cells expressing these lytic cycle indicators (Fig. 6E). These data demonstrate that the vCyc is
231 necessary to promote lytic gene expression in macrophages and that Rta is sufficient to drive
232 lytic gene expression in macrophages, illustrating how host and viral factors shape the outcome
233 of macrophage infection.

234 **DISCUSSION**

235 Myeloid cells, including macrophages, monocytes and dendritic cells, are well-documented
236 targets of γHV infection [11-27], though there remains little consensus on how infection is
237 regulated in these cells or why infection results in widely divergent outcomes. Here, we present
238 an in-depth analysis of MHV68 infection of macrophages, documenting multi-layered regulation
239 of outcomes. First, macrophages harvested early after MHV68 infection in vivo are
240 characterized by frequent transcription of the ORF75 locus in the absence of other detectable
241 viral RNAs. Second, MHV68 induces three divergent outcomes in a reductionist system of
242 macrophage infection: i) a restricted state of infection, reminiscent of latency, with infrequent
243 cells initiating lytic infection, ii) an abortive form of lytic replication or iii) full lytic replication.
244 Third, divergent infection outcomes are readily observed by manipulating virus (multiplicity of
245 infection, viral mutations) and host factors (cytokine exposure), illustrating how divergent
246 infection outcomes can occur in a single cell type. These data suggest that MHV68 replication in
247 macrophages is blocked at two stages, first a block in early transcription, overcome by high MOI
248 infection, and second, a block at virus DNA replication, overcome by IL-4 pre-treatment (Fig 4).
249 These studies further suggest a previously unappreciated role for the ORF75 locus as a
250 potentially important regulator of macrophage infection, and suggest re-evaluation of previous
251 assumptions (e.g. that macrophages poorly support lytic replication).

252 By examining the heterogeneity of macrophage infection at single cell resolution, our studies
253 provide a refined perspective of MHV68 infection in macrophages. These studies unequivocally
254 identify that MHV68 robustly infects macrophages and are capable of initiating transcription and
255 translation of at least the ORF73 gene, with only a minor fraction of these cells showing
256 hallmarks of lytic replication. Whether the majority of LANA+ cells reflect a bona fide latent
257 population or a previously undescribed, restricted form of infection remains an open question.
258 Although selective ORF75 transcription has not been reported in the context of MHV68
259 macrophage infection, transcripts mapping to the ORF75 locus have been observed in some in

260 vitro latency models, a finding previously attributed to potential detection of unspliced ORF73
261 transcripts [60-62]. Here, we detected individual ORF75 gene products (i.e. ORF75A, ORF75B,
262 and ORF75C) by polyA-based scRNA-seq, strongly suggesting that these RNAs represent
263 ORF75-specific transcripts, not unspliced ORF73 RNA. These findings further suggest that
264 ORF75 transcription is regulated in additional ways beyond those observed for lytic replication
265 [46]. Notably, ORF75 transcription has been reported in contexts beyond lytic replication for
266 EBV BNRF1 (the ORF75 ortholog), where it is expressed in lymphoblastoid cell lines [41], and
267 for KSHV ORF75, where it is detected in Kaposi's sarcoma lesions [63, 64]. Recent studies
268 have shown that the KSHV ORF75 promoter is regulated in a cell type-specific manner, active
269 in endothelial cells but repressed in B cells [40]. Collectively, these findings suggest that the
270 ORF75 locus may be subject to macrophage-specific regulation, that ORF75 gene products
271 may have unique functions in macrophages, and that ORF75-targeted interventions (e.g.
272 vaccination against ORF75-derived T cell epitopes [65-67]) may selectively disrupt macrophage
273 infection.
274 Through use of a reductionist system of macrophage infection, we find that MHV68 infection
275 can result in three divergent outcomes. Using infection with an intermediate infectious dose
276 (MOI=1), MHV68 readily infects the majority of cells, defined by LANAβlac expression, with only
277 a minor fraction of cells characterized by lytic protein expression and no measurable viral DNA
278 replication or infectious virus production; this finding parallels our in vivo analysis. While we can
279 detect LANAβlac+ J774 cells for up to 14 dpi, whether this in vitro model represents bona fide
280 latency remains unknown at this time. In striking contrast to intermediate dose infection,
281 infection with a high virus dose (MOI=10) greatly increases the frequency of cells initiating lytic
282 cycle transcription, with minimal viral DNA replication infectious virus production and a high rate
283 of cell death, findings strongly suggestive of abortive replication. The significant induction of
284 early transcription that occurs with a high MOI suggests that macrophage infection is subject to

285 at least two sequential levels of regulation: i) a block that limits entry into the lytic cycle
286 (observed with an intermediate infection dose) that can be overcome by a high MOI, and ii) an
287 additional block that prevents viral DNA replication and lytic replication following infection with a
288 high MOI, potentially due to activation of cell death pathways. Despite these barriers to lytic
289 replication, it is notable that pre-treatment with the cytokine IL-4 induces a high frequency of
290 lytic transcription, viral DNA replication and infectious virus production, consistent with previous
291 reports that IL-4 can promote virus replication in macrophages [55].
292 By investigating the interplay between viral and host factors in macrophage infection, our
293 studies demonstrate significant heterogeneity in infection outcome in macrophages. These
294 findings provide an important new perspective on previously published findings and help to
295 resolve previously ambiguities in the literature. First, the magnitude of MHV68 lytic replication
296 within bone marrow macrophages or myeloid cells is relatively modest compared to fibroblasts
297 [25, 68], with lytic antigen detected in a subset of bone marrow-derived macrophages and
298 RAW264.7 macrophages [30, 37, 55]. Our data are consistent with this and emphasize that
299 cells initiating lytic transcription represents only a fraction of infected cells. Second, there are
300 numerous studies that have identified positive and negative regulators of macrophage infection.
301 MHV68 lytic replication in macrophages is supported by multiple viral proteins (viral protein
302 kinase [24], vRCA [25], vCyclin, Rta) and host factors (H2AX [38], ATM [69] and apolipoprotein
303 E [70]). Parasitic infection can further promote macrophage infection through two distinct
304 mechanisms, either by eliciting IL-4 or IL-13, STAT6-inducing cytokines that directly
305 transactivate the MHV68 gene 50 promoter [37], or by expanding the number of large peritoneal
306 macrophages allowing for an increased frequency of infection targets in vivo [71, 72].
307 Conversely, MHV68 replication in macrophages is limited by type I and type II interferons [73],
308 IRF1 [74], HDAC1 and 2 [75], liver X receptors [35], and Low-Density Lipoprotein Receptor [36].
309 In vivo, IFNγ constrains MHV68 reactivation from latency within peritoneal macrophages [76]
310 and CD4 T cells constrain chronic macrophage infection in the lung [68]. Based on our current

311 findings, we postulate that these diverse regulatory mechanisms may affect the relative
312 proportion of cells initiating lytic replication with MHV68, or may fundamentally alter the
313 susceptibility of infection across all cells. Defining how these regulatory mechanisms influence
314 the frequency and outcome of macrophage infection at the single-cell level remains an
315 important future goal.

316 This study has important limitations. First, our studies of primary in vivo infection focus on a
317 single, early timepoint. Conservatively, we can conclude that the high frequency of LANA+
318 macrophages with detectable ORF75 transcripts is not explained by the current paradigm of
319 lytic or latent transcription (e.g. exemplified by [49]) and suggests additional mechanisms of
320 transcriptional regulation within the ORF75 locus beyond that in fibroblasts [46]. Second, our in
321 vitro studies use the J774 mouse myeloid cell line, a reductionist in vitro system to study
322 MHV68-macrophage interactions. Though these cells demonstrate parallels with primary
323 macrophages (e.g. infrequent lytic replication at baseline that can be potently enhanced by IL-4
324 pretreatment), whether the precise molecular mechanisms engaged in these cells reflect one or
325 more primary macrophage subsets remains to be determined. This is an important, but
326 challenging question, given that macrophage subsets in vivo are known to respond differently to
327 infection (e.g. large versus small peritoneal macrophages differ in their infection frequency with
328 MHV68 early after infection [71, 72]; infection of marginal zone macrophages is thought to
329 precede B cell latency [14, 33], whereas subcapsular sinus macrophages limit infection [34]).
330 Despite these limitations, our results are consistent with previous studies demonstrating lytic
331 protein expression in a subset of bone marrow-derived macrophages and RAW264.7
332 macrophages [30, 37, 55], and revealing that high MOI can overcome genetic requirements for
333 lytic gene expression at a lower MOI [38]. Finally, it is important to recognize that the outcome
334 of γHV-myeloid cell infection may be affected by the mode of virus entry. While our experiments
335 test macrophage infection using cell-free virus, additional modes of infection have been reported
336 (i.e. virus internalization via epithelial cell presentation [31], or infection through an Fc receptor-

337 dependent mechanism [30]). These factors would likely be influenced by the route and stage of
338 infection and host immune status.

339 In total, our studies provide critical new insights into how γHV infection of myeloid cells is
340 regulated, demonstrating unanticipated transcription during primary infection in vivo and three
341 divergent infection outcomes which can be readily manipulated by virus and host factors. Our
342 studies highlight how bulk analyses and subsequent conclusions drawn from these analyses are
343 insufficient to describe the heterogeneity of MHV68 infection in myeloid cells – a conclusion that
344 could apply to γHV interactions beyond the myeloid compartment. These data redefine a
345 conceptual framework to study myeloid cells as a γHV target and emphasize the knowable
346 complexity of γHV-myeloid cell interactions.

347 **METHODS**

348 **Viruses and Tissue Culture**

349 Mouse 3T12 fibroblasts (ATCC CCL-164), mouse J774A.1 macrophages ("J774"; ATCC
350 TIB-67), and mouse RAW264.7 macrophages (ATCC, TIB-71) were cultured in complete DMEM
351 (cDMEM): Dulbecco's modified Eagle medium (DMEM; Life Technologies) supplemented with
352 5% and 10% fetal bovine serum (FBS; Atlanta Biologicals) respectively, 2 mM L-glutamine, 10
353 U/mL penicillin, and 10 µg/mL streptomycin sulfate. Cells were cultured at 37°C with 5% CO_2.
354 Wild-type (WT) MHV68, MHV68.LANA::βlac, MHV68.H.GFP [50], MHV68.ORF59.GFP [51],
355 MHV68.vCycKO [56], MHV68.CA-RTA [77] and MHV68.vCyc::blac viruses were grown and
356 prepared as described previously [43, 44, 50], with virus titers determined from at least three
357 independent plaque assays. MHV68.vCyc::blac was created through BAC recombineering,
358 introducing a C-terminal fusion with the blac gene downstream of the endogenous vCyc
359 (ORF72) gene (manuscript in submission, Noell et al).

360

361 **Infection**

362 All in vitro infections were based on live cell counts with the TC20 Automated Cell
363 Counter (Bio-Rad) with Trypan Blue dye (Bio-Rad, Cat. No. 145-0021). Viral stock was diluted
364 with cDMEM for viral inoculum with a multiplicity of infection (MOI) of 1 or 10 PFU/cell. Cells
365 were incubated at 37°C with 5% CO_2 for 1 hour, with rocking every 15 min, before viral inoculum
366 was removed and replaced with 1mL of cDMEM. For qPCR analysis of viral DNA replication and
367 for beta-lactamase staining and flow cytometric analysis of infected cells, viral inoculum was left
368 on cells after 1 hr infection time. For IL-4 treatments, media containing recombinant mouse IL-4
369 (PeproTech, Cat. No. 214-14) was added to cells 16 hours before infection. Following infection,
370 media containing 0, 10 or 100ng/mL of fresh IL-4 containing media were added respectively.
371 Samples were harvested at the indicated hours post-infection (hpi) through either cell scraping
372 (for DNA isolation) or through incubation in TRIzol (for RNA isolation).

373

374 **Plaque Assay**

375 Plaque assay quantification of viral titer was performed using 3T12 cells. Cells were
376 plated in 12-well plates at 8.5×10^4 cells per well one day prior to infection. Viral samples were
377 diluted 10-fold in 5% cDMEM. An internal standard was included for each infection to ensure
378 reproducible sensitivity for each plaque assay. Cells were incubated with virus for 1 hour at
379 37°C with 5% CO_2. Plates were rocked every 15 min. Cells were then covered with an overlay
380 composed of a 1:1 mix of 10% cDMEM and carboxymethyl cellulose (CMC; Sigma, Cat. No. C-
381 4888) supplemented with Gibco™ Amphotericin B (Thermo Fisher Scientific, Cat. No.
382 15290018). Cells were incubated for 8 days before staining with 0.5% methylene blue and
383 plaques were counted.

384

385 **RT-qPCR**

386 RNA was isolated from infected cells harvested at indicated times by 10-minute
387 incubation in TRIzol® reagent (Thermo Fisher Scientific, Cat. No. 15596026), followed by
388 TURBO™ DNase (Invitrogen, Cat. No. AM2238) treatment according to manufacturer's
389 protocols. RNA amplification and removal of DNA was confirmed by PCR amplification of the
390 control host gene, 18S, in the presence or absence of reverse transcriptase. RNA presence and
391 absence of DNA was confirmed with RT-PCR and PCR respectively. RT-PCR was performed
392 using the OneStep RT-PCR kit (Qiagen, Cat. No. 210212) with the following conditions: (i) 50°C
393 for 30 min, (ii) 95°C for 15 min, (iii) 40 cycles of 94°C for 30 sec, 52°C for 30 sec, and 72°C for
394 30 sec, (iv) 72°C for 10 min, and (v) hold at 4°C. PCR was performed using *Taq* DNA
395 polymerase (Qiagen, Cat No. 201205) with the following conditions: (i) 95°C for 5 min, (ii) 40
396 cycles of 94°C for 30 sec, 52°C for 30 sec, and 72°C for 30 sec, (iii) 72°C for 10 min, and (iv)
397 hold at 4°C. RNA samples that showed no product following PCR amplification were deemed
398 DNA-free, and then converted to cDNA using random primers (250ng/uL) (Invitrogen, Cat. No.

399 48190011) and SuperScript II reverse transcriptase (Invitrogen, Cat. No. 18064014) following
400 the manufacturer's protocol. 100 nanograms of cDNA was used for qPCR analysis of the
401 identified genes (Quantitect Primer Assay, Qiagen) using the iQ SYBR green supermix (BioRad
402 Cat. No.1708880) with the following conditions: (i) 95°C for 3 min, (ii) 40 cycles of 95°C for 15
403 sec, 60°C for 1 min, and (iii) 95°C for 15 sec, 60°C for 1 min, and 95°C for 15 sec. Amplification
404 of viral genes was normalized to murine 18S expression to calculate the relative difference of
405 target gene expression using the Pfaffl method, as previously described [6, 78] : Target primer
406 efficiency^TargetΔCt/18S primer efficiency^18$S\Delta Ct$. A single product for each target was
407 confirmed by melt curve analysis. PCR primers are listed in **Table 1.**
408
409 **Quantitative PCR for quantification of viral DNA replication**
410 Infected cells were harvested by cell scraping at time (hpi) indicated. Harvested cells
411 underwent three freeze/thaw cycles and DNA was isolated using the DNeasy Blood and Tissue
412 Kit (Qiagen, Cat. No. 69504), with an overnight proteinase K incubation and heat inactivation at
413 56°C. DNA was normalized to a concentration of 20 ng/uL in molecular grade water. qPCR
414 analysis was done on 100ng of DNA using a LightCycler 480 Probe Master-Mix kit (Roche, Cat.
415 No. 04707494001) and a primer and probe set specific to MHV68 glycoprotein B (gB) to
416 quantify the number of viral genome copies. Viral genome copies/cell concentration was
417 determined by dividing gB quantity over NFAT5 quantity. Primers and probes listed in Table 1. A
418 gB or nuclear factor of activated T cells 5 (NFAT5) [79, 80] standard curve was generated using
419 a gB or NFAT5 plasmid dilution series ranging from 10^2 to 10^{10} copies diluted in background
420 DNA, with a limit of detection (LOD) of 100 copies.
421
422 **Single-cell RNA Sequencing**
423 To characterize MHV68 transcription during primary, acute peritoneal macrophage
424 infection *in vivo*, female C57BL/6 mice were infected with $1x10^6$ PFU by intraperitoneal injection.

425 Peritoneal cells were harvested 16 hours post-infection, stained with the live/dead discrimination
426 dye Zombie Near-IR (Zombie NIR™, BioLegend, Cat. No. 423105), F4/80-AlexaFluor 674
427 (clone BM8, 1:200 dilution) in the presence of Fc receptor blockade (clone 2.4G2), and CCF2-
428 AM (Thermo Fisher, Cat. No. K1023). Cells were sorted on a MoFlo Astrios, purifying live,
429 single, F4/80+ cells that either had CCF2 cleavage (indicating virus infection, defined by
430 expression of the LANA::blac fusion protein) or lacking CCF2 cleavage (indicating cells that
431 were not infected or failed to express the LANA::blac fusion protein). Single cell RNA-seq was
432 prepared using the Chromium 3' V3 library kit (10X Genomics). Cell processing and sequencing
433 was performed by the University of Colorado Cancer Center Genomics Shared Resource
434 (RRID: SCR_021984). Resulting data were processed as follows: Cell Ranger (v6.0.1) [81] was
435 used to process the fastq files to cell and gene count tables using unique molecule identifiers
436 (UMIs) with the include-introns parameter. Because of the difficulties counting viral reads, this
437 was performed in a two-pass manner. In the first pass, reads were aligned to a chimeric
438 genome of mouse mm10 (GENCODE M23 gene annotations) and MH636806.1 (no gene
439 annotations, only positive and negative strand alignment). The viral counts were stored in
440 metadata and removed from the counts matrix. Reads mapping to MH636806.1 in step 1 were
441 aligned to the same chimeric genome but in this case, the viral transcriptome as well as specific
442 intergenic regions were annotated. The intergenic regions were determined as the strand-
443 specific sequences between genes with 1 base pair of padding on both ends. To minimize reads
444 overlapping with multiple viral genes, only the first 70bp of each read were aligned and counted.
445 The resulting counts matrix of viral alignment was appended to the host gene counts from step
446 1.
447 The Seurat (v4.0.4) [82] pipeline was used for downstream quality control and analysis.
448 Cellranger-filtered data was read into Seurat. Host genes were removed if identified in fewer
449 than 10 cells while viral gene and intergenic regions were removed if found in no cells. Cells
450 were removed if they expressed < 50 genes or viral regions, < 5000 UMIs, > 5 % total UMIs

451 from mitochondria, or > 70000 UMIs. The filtered data was normalized by dividing gene counts
452 by total counts per cell and multiplied by 10,000 followed by natural-log transformation. The top
453 2,000 most variable genes were scaled with total UMI and percentage mitochondria regressed
454 out. These were used to calculate principal components (PCs) with the top 20 used to perform
455 Uniform Manifold Approximation and Projection (UMAP) and determining the k-nearest
456 neighbors and clustering.
457 Clusters were identified by over-representation analysis and examining the top enriched
458 markers. Canonical cell type markers were plotting in UMAP space and using dot plots. Dot
459 plots, bar plots, scatter plots, and violin plots were generated using Seurat and ggplot2 R
460 packages (v3.4.0) [83].
461
462 **Flow Cytometry**
463 3T12 and J774 cells were infected with MHV68 LANAβlac or MHV68.H.GFP at an MOI
464 of 1 PFU/cell and harvested at the indicated time points followed by staining for flow cytometric
465 analysis. Samples treated with the recombinant murine IL-4 were given 10% cDMEM with
466 10ng/mL of IL-4 eighteen hours prior to infection and replaced with fresh media containing IL-4
467 immediately following infection. Cell suspensions were stained with LIVE/DEAD fixable Near-IR
468 Dead Cell stain kit (Invitrogen, Cat. No. L10119) at a 1:1000 dilution in BSS wash (111mM
469 Dextrose, 2mM KH_2PO_4, 10mM Na_2HPO_4, 25.8 $CaCl_2$•$2H_2O$, 2.7mM KCl, 137mM NaCl, 19.7mM
470 MgCl•$6H_2O$, 16.6mM $MgSO_4$). Cells were then stained for CCF2 or protein detection. Cells for
471 CCF2 detection were stained with CCF2-AM (Thermo Fisher, Cat. No. K1023) at a 1:10 dilution
472 following the manufacturer's protocol. To detect proteins, cells were stained with a Fc receptor
473 block (Fc Shield, Tonbo Biosciences, Cat. No. 70-0161), a rabbit antibody against the MHV68
474 ORF4 protein (vRCA, 1:400 dilution) (gift of the Virgin Lab, Washington University St. Louis [6,
475 84]) labeled with a Zenon R-phycoerythrin anti-rabbit IgG reagent (Invitrogen, Cat. No. Z25307),
476 per manufacturer's recommendations, and a AF647-conjugated anti-mouse phospho-histone

477 H2AX antibody (1:800 dilution) (clone JBW30). Samples were fixed in 1% paraformaldehyde
478 prior to analysis using the Bio-Rad ZE5/YETI Cell Analyzer or an Agilent Novocyte Penteon flow
479 cytometer. To detect actin mRNA, cells were stained with buffers and probes using the
480 PrimeFlow RNA assay kit (ThermoFisher), as previously published [6]. All flow cytometry
481 experiments included unstained, single-stain and full minus one controls to define background
482 fluorescence, fluorescent signal spread and compensation.
483
484 **Light microscopy**
485 At the indicated time points, 6-well plates of 3T12 or J774 cells were imaged on a Nikon
486 Eclipse Ti2 inverted light microscope equipped with Iris 15 camera (Photometris) and use of NIS
487 elements software. Plates were mounted on a stage heated to 37°C. A 10x phase objective was
488 used to capture brightfield images. Immediately following image acquisition, samples were
489 harvested and processed for flow cytometric analysis.
490
491 **Statistical Analysis and Software**
492 Data analysis, graphing and statistical analyses were performed using GraphPad Prism
493 (version 9.4.0; GraphPad Software, San Diego, California USA, www.graphpad.com). Flow
494 cytometry data were analyzed using FlowJo (version 10.8.1. Ashland, OR: Becton, Dickinson
495 and Company; 2022). scRNA-seq data processing and analysis were done as described above.
496 Statistical significance was tested by unpaired, nonparametric, Mann-Whitney t test or 1-way
497 ANOVA for comparing replicate values from experiments. Raw and processed single cell RNA-
498 Seq data is available through NCBI GEO (GSE233202).
499
500 **Cell Sorting**
501 J774 fibroblasts were infected at an MOI=1 with for one hour, after which inoculum was
502 removed. Cells were harvested at 48 hours post-infection (hpi) and stained with β-lactamase

503 substrate as previously reported [44] using the CCF2-AM substrate (Invitrogen, Life
504 Technologies). Cells were subjected to fluorescence activated cell sorting (FACS), with cells
505 gated on singlet cells that were positive for the cleaved CCF2-AM substrate (subsequently
506 referred to LANAβlac+ sorted cells). Cleavage of CCF2-AM was defined as positive
507 fluorescence in the 405-448/59nm emission channel obtained in WT MHV68.LANAβlac,
508 compared to parental WT MHV68 infected cultures with no beta-lactamase fusion gene, used to
509 define background fluorescence. β-lactamase positive cells were sorted using a Astrios EQ
510 (Beckham Coulter). Cells were either plated onto 6-well plates at 5 x 10^5 cells/mL, collected for
511 quantitative PCR or plaque assay measurement. The plated CCF2+ J774 cells were cultured at
512 37°C with 5% CO_2, grown in complete DMEM (cDMEM): Dulbecco's modified Eagle medium
513 (DMEM; Life Technologies) supplemented with 10% fetal bovine serum and passaged upon
514 confluency (typically every 3-4 days). Upon passaging, cells and supernatant were collected
515 followed by resuspension in 1mL of 10% cDMEM. Cell counts were measured by BIORAD
516 TC20 automated cell counter. At 7 days post sort (dps), one 6-well of cells was collected and
517 resuspended in 1mL of 10% cDMEM and flow cytometry for CCF2 detection was performed with
518 700uL of the resuspended cells. At 14 dps, one 6-well of cells was collected and resuspended in
519 1mL of 10% cDMEM and flow cytometry for CCF2 detection and viral protein vRCA and H2AX
520 was performed with 700uL of the resuspended cells (See Flow Cytometry Methods Section). At
521 both 7 and 14 dps 300uL of the 1mL collected cells were used for qPCR and plaque assay
522 analysis.
523
524 **Ethics Statement**
525 All animal studies were performed in accordance with the recommendations in the Guide
526 for the Care and Use of Laboratory Animals of the National Institutes of Health. Studies were
527 conducted in accordance with the University of Colorado Denver/Anschutz Institutional Animal
528 Use and Care Committee under the Animal Welfare Assurance of Compliance policy

529 (assurance no. D16-00171). All procedures were performed under isoflurane anesthesia, and all

530 efforts were made to minimize suffering.

531 **Figure Legends**

532

533 **Figure 1. Single cell RNA sequencing analysis of acute MHV68 macrophage infection.**
534 C57BL/6J mice were infected with $1x10^6$ PFU of WT MHV68.LANAblac virus. MHV68-infected,
535 LANAblac+ peritoneal cells were sort-purified at 16 hpi and subjected to scRNA-seq analysis.
536 **(A-B)** Visualization of cell types based on lineage marker genes depicted in panel B. **(C)**
537 Quantification of cell subsets defined by scRNA-seq. **(D)** UMAP visualization of cells with at
538 least 1 viral UMI detected per cell identified by purple. **(E)** Frequency of cells stratified by the
539 fraction of viral UMIs out of total UMIs detected per cell. 56 cells had >0.1% of total UMIs
540 contributed by viral UMIs, including 23 of 9101 macrophages (0.25%), 25 of 25 macrophages
541 with lytic gene expression (100%) and 8 of 70 dendritic cells (11.43%). Data are from 9,537
542 cells. Supporting data in **Fig S1-S2**.

543

544 **Figure 2. Single cell RNA sequencing analysis of acute MHV68 macrophage infection**
545 **reveals two distinct transcriptional profiles.** Analysis of viral gene expression defined by
546 scRNA-seq in macrophage subsets from **Figure 1. (A-C)** Frequency of cells with detectable
547 reads mapping to MHV68 genes, comparing (A) macrophages (82.79% viral UMI+), (B)
548 macrophages with proliferative gene signature (52.08% viral UMI+), or (C) macrophages with
549 lytic gene expression (100% viral UMI+). Viral genes are indicated on the x axis, arranged from
550 left to right based on the published MHV68 genome, with the frequency of cells positive for each
551 viral gene depicted on the y axis. To facilitate comparison of gene expression across the viral
552 genome and cell populations, circles are color-coded to identify values that are in the indicated
553 ranges (defined in key, panel A). Dotted lines indicate different thresholds of viral gene
554 positivity, empirically defined. For panel C, only genes with >75% positivity were color-coded,
555 given the limited number of cells and high viral positivity. **(D)** Frequency among macrophages

556 defined by detection of ORF73, ORF75A, ORF75B, and ORF75C RNAs, enumerating all
557 potential gene combinations for macrophages from panels A-C.
558
559 **Figure 3. MHV68 readily infects J774 macrophages with limited lytic transcription.**
560 Analysis of MHV68 infection (WT MHV68.LANAblac, MOI=1 PFU/cell) comparing 3T12
561 fibroblasts and J774 macrophages. **(A)** Representative brightfield images of infected 3T12 (top)
562 or J774 cells (bottom) early (24 hpi, left) or late (72 hpi, right) post-infection. 3T12 cells showed
563 cytopathic effect (CPE), including cell rounding (24 hpi) and monolayer destruction (72 hpi), in
564 contrast to J774 cells. **(B)** Viral DNA quantitation defined by qPCR. **(C)** Virus replication defined
565 by plaque assay. **(D-E)** Frequency of MHV68-infected, LANAβlac+ cells defined by flow
566 cytometry, detected by CCF2 substrate cleavage, analyzing single, viable cells. Samples
567 infected with WT MHV68 (left, panel E) define background signal and do not encode LANAβlac.
568 **(F-G)** Quantitation of viral gene expression defined by qRT-PCR, comparing 3T12 and J774
569 cells at 24 hpi (left) or J774 cells at 24 and 48 hpi (right). Flow cytometric analysis focused on
570 single, viable cells. Data depict mean ± SEM, from 3 independent experiments with 3 biological
571 replicates per experiment (B, D, F-G) or 2 (t=0) or 6 (t=24, 48 hpi) independent experiments (C),
572 with individual symbols representing independent biological samples. Statistical analysis was
573 done using unpaired t test, with statistically significant differences indicated, *$p<0.05$, **$p<0.01$,
574 ***$p<0.001$, ****$p<0.0001$.
575
576 **Figure 4. Only rare MHV68 infected macrophages display lytic gene expression.** Analysis
577 of MHV68 infection and lytic cycle profiles with either MHV68.H.GFP or MHV68.LANAblac
578 (MOI=1 PFU/cell) comparing 3T12 fibroblasts and J774 macrophages. **(A)** Flow cytometric
579 analysis of virus-expressed GFP in 3T12 or J774 cells 18 hpi. Data depict the frequency of cells
580 with GFP expression, an indicator of MHV68.H.GFP infection. Background fluorescence defined
581 by WT MHV68.LANAblac-infected cells (left column), without the addition of the CCF2

582 fluorescent substrate. **(B)** Frequency of HygroGFP+ cells defined by flow cytometry, as in panel
583 A. **(C)** Frequency of vCycblac+ cells defined by flow cytometry. **(D)** Flow cytometric analysis of
584 lytic infection-associated proteins, vRCA and gH2AX in 3T12 (top) or J774 (bottom) cells,
585 comparing mock (left) or WT MHV68.LANAblac-infected cells. Data for 3T12 cells at 48 hpi was
586 not assessed due to extensive cell destruction. **(E)** Quantification of the frequency of infected
587 cells with protein expression associated with lytic infection defined by flow cytometry, as in
588 panel D. Flow cytometry data focus on single, viable cells defined using gating strategies in **Fig.**
589 **S3A, S4B**. Data show mean ± SEM from 3 experiments, with 2 (B,E) or 3 samples (C) per
590 experiment. Statistical analysis done using Mann-Whitney test, with statistically significant
591 differences as indicated, **$p<0.01$, ****$p<0.0001$.
592
593 **Figure 5. High dose MHV68 infection results in abortive replication.** MHV68 outcomes in
594 J774 macrophages comparing intermediate (MOI=1 PFU/cell) or high dose (MOI=10) infection.
595 **(A)** Flow cytometric analysis of GFP in MHV68.LANAblac- (left; negative control with no CCF2
596 substrate) or MHV68.H.GFP-infected cells (right) at MOI=1 (top) or MOI=10 (bottom). **(B)**
597 Frequency of GFP+ cells quantified by flow cytometry, as in A. **(C)** Frequency of ORF59GFP+
598 J774 cells quantified by flow cytometry at 24 or 72 hpi. **(D)** Flow cytometric analysis of actin
599 mRNA levels 24 hpi in mock or WT MHV68-infected cells with individual rows showing
600 independent biological samples. **(E)** Quantitation of viral RNA expression by qRT-PCR
601 standardized to 18S RNA, comparing intermediate or high MOI (MHV68.LANAblac) at the
602 indicated timepoints. **(F)** Frequency of MHV68.HygroGFP-infected single cells that are viable,
603 quantified by flow cytometry. **(G)** Quantitation of viral DNA by qPCR in J774 (left) or 3T12 cells
604 (right) as a function of MOI (MHV68.LANAblac). **(H)** Infectious virus production quantified by
605 plaque assay, comparing 3T12 cells (MOI=1) with J774 cells (MOI=1 or 10). Flow cytometry
606 data analyzed single, viable cells (A-D) or single cells (F), with gating strategy in **Fig. S3**. Data
607 show mean ± SEM, with individual symbols showing independent biological samples from 2-3

608 independent experiments with 2-3 biological replicates per experiment. Statistical analysis was
609 done using Mann-Whitney test with statistically significant differences indicated, **p<0.01,
610 ***p<0.001.
611
612 **Figure 6. MHV68 infection of macrophages is modulated by host and viral factors.** All
613 infections done with MOI=1. **(A-D)** IL-4 effect on MHV68 infection and genome replication in
614 J774 macrophages. IL-4 cultures were pretreated with IL-4 for 16-18 hours at the indicated
615 concentration, with fresh IL-4 replenished after infection. **(A)** Flow cytometric analysis of
616 MHV68.H.GFP infection in 3T12 (top), untreated J774 (middle) or IL4-treated J774 cells at 24
617 (left) or 48 hpi (right), analyzing single, viable cells. **(B)** Frequency of GFP+ cells quantified by
618 flow cytometry, as in A. **(C-D)** IL-4 effect on viral DNA replication **(C)** and infectious virus
619 production **(D)** in WT MHV68-infected J774 cells. **(E)** Frequency of J774 cells expressing
620 markers of lytic infection (gH2AX, vRCA) quantified by flow cytometry, comparing WT, vCycKO
621 or CA-RTA MHV68 at 24 or 48 hpi. Flow cytometric analysis focused on single, viable cells.
622 Data depict mean ± SEM, with individual symbols representing independent biological samples
623 from 2-3 independent experiments with 2-3 biological replicates per experiment (B,C,E) or from
624 1-2 independent experiments with 3 biological replicates measured (D). Statistical analysis used
625 (B) unpaired t test, (C) one-way ANOVA comparing samples collected at the same timepoint
626 untreated versus cytokine treated, or (E) one-way ANOVA comparing samples collected at the
627 same timepoint with WT infection (nonparametric Kruskal-Willis test subjected to Dunn's
628 multiple comparison test), with statistically significant differences indicated, *p<0.05, **p<0.01,
629 ****p<0.0001.

630 **Table 1:** *Oligonucleotides for RT-PCR, PCR, and qPCR analysis*

Name	Accession number and Genome Position *	Sequence	Purpose
gB Forward Primer	MHV68: 17873…17892	5'—GGC CCA AAT TCA ATT TGC CT—3'	TaqMan qPCR for MHV68 genome
gB Reverse Primer	MHV68: 17924…17943	5'—CCC TGG ACA ACT CCT CAA GC—3'	TaqMan qPCR for MHV68genome
gB Probe	MHV68: 17896…17921	5'—ACA AGC TGA CCA CCA GCG TCA ACA AC—3'	TaqMan qPCR for MHV68genome
NFAT5 Probe	NC_000074.7 (108020072..108106149)	5'—ACG AGG TAC CTC AGT GTT—3'	TaqMan qPCR for murine genome
NFAT5 Forward	NC_000074.7 (108020072..108106149)	5'—CAT GAG CAC CAG TTC CTA CAA TGA T—3'	TaqMan qPCR for murine genome
NFAT5 Reverse	NC_000074.7 (108020072..108106149)	5'—TGC TTT GGA TTT CGT TTT CGT GAT T—3'	TaqMan qPCR for murine genome
18S Forward Primer	Accession Number: NR_003278	5'— AGA TCA AAA CCA ACC CGG TGA—3'	RT-PCR and PCR for murine 18S gene
18S Reverse Primer	Accession Number: NR_003278	5'—GGT AAG AGC ATC GAG GGG GC—3'	RT-PCR and PCR for murine 18S gene
ORF73 SYBR G – Forward Primer	MHV68: 104092…104073	5'— GAG CCC CCT ACA GAG CCC CC —3'	SYBR Green qPCR for MHV68ORF73 gene
ORF73 SYBR G-Reverse Primer	MHV68: 103981…104000	5'— CAC CTT GCT CTG CAC CGG CA —3'	SYBR Green qPCR for MHV68ORF73 gene
ORF6 SYBR G – Forward Primer	MHV68: 11699…11783	5'— ATG TTG TCA GCA CCC ATG AA—3'	SYBR Green qPCR for MHV68ORF6 gene
ORF6 SYBR G – Reverse Primer	MHV68: 11802…11783	5'— AAG GGC AGT AGC TGG TCA GA—3'	SYBR Green qPCR for MHV68ORF6 gene
M7 SYBR G – Forward Primer	MHV68: 70109…70128	5'—GCT CCT GCT GAC ACA TCA GA—3'	SYBR Green qPCR for MHV68M7 gene
M7 SYBR G – Reverse Primer	MHV68: 70185…70166	5'—TGG GGT TTG GAC TCT GTA GG—3'	SYBR Green qPCR for MHV68M7 gene
MHV68 ORF75A iQ SYBR - Forward Primer	MHV68: 114964…114945	5'—ACC TGA CAC CCC AAG AAC AG—3'	SYBR Green qPCR for MHV68ORF75A gene
MHV68 ORF75A iQ SYBR - Reverse Primer	MHV68: 114834…114853	5'—GAG CAC TTT TGG TGG AGA GC—3'	SYBR Green qPCR for MHV68ORF75A gene
MHV68 ORF75B iQ SYBR - Forward Primer	MHV68: 113267…113248	5'—CAG CCT CTC AAC CTT TCC AG—3'	SYBR Green qPCR for MHV68ORF75B gene

MHV68 ORF75B iQ SYBR - Reverse Primer	MHV68: 113093…113112	5'—ATA GGA GCC ACC GTT GAT TG—3'	SYBR Green qPCR for MHV68.ORF73βla ORF75B
MHV68 ORF 75C iQ SYBR - Forward Primer	MHV68: 109930…109911	5'—AAG ACA CAG AGG CTG GGA GA—3'	SYBR Green qPCR for MHV68ORF75C gene
MHV68 ORF75C iQ SYBR - Reverse Primer	MHV68: 109758…109777	5'—GAC GGG TAG ACG TGG TGA CT—3'	SYBR Green qPCR for MHV68ORF75C gene
BLAC SYBR G – Forward Primer	MHV68.ORF73βla: 104867…104886	5'—GCT ATG TGG CGC GGT ATT AT—3'	SYBR Green qPCR for MHV68.ORF73βla Blac gene
BLAC SYBR G – Reverse Primer	MHV68.ORF73βla: 104701…104720	5'—AAG TTG GCC GCA GTG TTA TC—3'	SYBR Green qPCR for MHV68.ORF73βla Blac gene

MHV68 genome coordinates refer to NC_001826. In the case of MHV68.ORF73βla Bla gene, sequences correspond to NCBI GenBank: MH636806.1, the complete genome sequence of MHV68 containing the ORF73bla gene fusion.

635 **Supplemental Figure Legends**

636

637 **Figure S1. Single cell RNA sequencing analysis of acute MHV68 macrophage infection.**
638 Data correspond to **Figure 1**. (A) Visualization of gene expression based on UMAP topography
639 in Fig. 1A. Maximal expression is designated by purple, with absence of detection designated by
640 gray. Each panel depicts a distinct lineage-defining gene used to identify cell types in Fig. 1,
641 with signature genes for each cell type as follows. Macrophage: Adgre1 (encodes the F4/80
642 protein), Itgam (encodes the CD11b protein). Macrophage proliferative: Top2a, Mki67.
643 Macrophage lytic: ORF54, ORF7. B cell: Cd19, CD79a. Monocyte: Ly6c2, Ccr2. Dendritic cell:
644 Itgax, H2-Ab1. T cell: Cd3d, Thy1. (B-E) scRNA-seq quality control metrics across cell subsets,
645 including (B) UMI Count, (C) Features, (D) % mitochondrial reads, and (E) S score, a
646 proliferation-associated gene signature.

647

648 **Figure S2. Single cell RNA sequencing analysis of acute MHV68 macrophage infection**
649 **analyzed using a higher number of cell clusters.** Data correspond to **Figure 1**, with scRNA-
650 seq analyzed as 14 clusters. **(A)** UMAP visualization of clusters. **(B)** Visualization of the
651 frequency and magnitude of host gene expression across clusters, with cell type designation
652 indicated on right. **(C-F)** Quality control metrics across the 14 clusters, including (C) UMI Count,
653 (D) Features, (E) % mitochondrial reads, and (F) S score, a proliferation-associated gene
654 signature. **(G)** UMAP visualization of cells with at least 1 detectable viral UMI per cell identified
655 in red. **(H)** Frequency of cell subsets stratified by the frequency of viral UMIs of total UMIs
656 detected per cell. **(I-J)** Percentage of viral UMIs out of total UMIs across clusters (panel I, y axis
657 range from 0-50%), or (J) which is the same as S2I but excluding 56 cells with viral UMIs >
658 0.1%. Data are from 9,537 cells, with clusters containing between 25-2,532 cells. Panel G is
659 included to provide a frame of reference and depicts the same data as in Figure 1D.

660

661 **Figure S3. Flow cytometry gating strategy and viral gene expression during MHV68**
662 **infection. (A)** Flow cytometry gating strategy to analyze MHV68-infected cells, in support of
663 **Figure 3E**. 3T12 cells infected with MHV68 LANAblac or WT.MHV68.H.GFP were analyzed by
664 flow cytometry, using sequential focused analysis (i.e. ”gating”) to consider cells that are single
665 cells (defined sequentially as “Singlets by SSC” and “Singlets by FSC”) that are viable (”Live
666 cells”) defined by exclusion of a dye that identifies dead cells. Live cells were then analyzed for
667 GFP fluorescence as measured by the GFP detection channel. Cells infected with
668 MHV68.LANAblac, without additional of the CCF2 fluorescent substrate, identified background
669 fluorescence, in contrast to samples infected with MHV68.H.GFP which encoded GFP. Controls
670 included single-stained samples with only one stain to define the bounds of a gate for the
671 fluorophore of interest. **(B-D)** Viral gene expression defined by qRT-PCR in 3T12 or J774 cells
672 infected with WT MHV68.LANAblac (MOI=1) at 16 hpi (B,D) or 24 hpi (C) in support of **Figure**
673 **3F-G**. Data show mean ± SEM from 3 independent experiments with 3 biological replicates
674 measured in technical triplicates per experiment (depicted by individual symbols) (B,D) or from 1
675 experiment with 3 biological replicates measured in technical triplicates, with ORF73 data from
676 Fig. 2B (C). Statistical analysis was done using unpaired t test with statistically significant
677 differences as indicated. ** $p<0.01$, ***$p<0.001$, ****$p<0.0001$. ns, no statistical significance
678 detected.
679
680 **Figure S4. Gating of flow cytometry analysis of MHV68 LANAβlac infected J774 cells for**
681 **lytic protein markers. (A)** Analysis of GFP expression in 3T12 fibroblasts, J774 and
682 RAW264.7 macrophage cell lines at 24 or 48 hpi, following infection with MHV68.H.GFP
683 (MOI=1). **(B)** Gating strategy to analyze vRCA and gH2AX expression in MHV68-infected J774
684 cells, in support of **Figure 4C**. Cells were analyzed by flow cytometry, using sequential focused
685 analysis (i.e. ”gating”) to consider cells that are single cells (defined sequentially as “Singlets by
686 SSC” and “Singlets by FSC”) that are viable (”Live cells”) defined by exclusion of a dye that

687 identifies dead cells. Live cells were then analyzed for antibody binding for lytic protein markers.
688 Gate boundaries were defined using a combination of “single stain” samples, containing only the
689 fluorophore of interest, and “full minus one” controls, lacking the antibody in the fluorescent
690 channel of the excluded fluorophore (not shown). **(C-I)** Analysis of MHV68-infected, FACS-
691 purified J774 cells over time. **(C)** Experimental overview with J774 macrophages infected with
692 MHV68.LANAblac (MOI=1), followed by sorting for LANAblac+ cells defined based on CCF2
693 substrate cleavage. Mock and LANAblac+ sorted cells were cultured and analyzed over 14
694 days. **(D)** Total cell counts over the course of the study, with each vertical line indicate a
695 subsequent cell passage. **(E)** Flow cytometric analysis of LANAβlac expression defined by
696 cleavage of the CCF2 fluorescent beta-lactamase substrate, analyzing single, viable cells, with
697 values in the right gate defining the frequency of cells with CCF2 substrate cleavage. **(F)**
698 Quantification of LANAβlac+ cell frequency defined by flow cytometry, as in panel E. **(G)** Flow
699 cytometric analysis of MHV68 lytic cycle-associated proteins (vRCA, gH2AX) at 14 dps,
700 comparing mock (left) or CCF2-sorted, LANAblac+ cells (right). Data depict events that were
701 single, viable cells, with values defining the frequency of cells with vRCA and/or phosphorylated
702 host γH2AX, indicative of lytic MHV68 infection, as in panel B. **(H)** Frequency of vRCA+
703 gH2AX+ cells defined by flow cytometry, as in panel G. **(I)** Quantitation of viral DNA by qPCR.
704 Dotted line indicates mean 3T12 viral genome copies/cell at 72 hpi. Data show mean ± SEM
705 from 3 independent experiments with 3 biological replicates per experiment (depicted by
706 individual symbols) (A) or from 2 independent experiments.

Acknowledgments:

We thank Dr. Brian Russo's lab, especially Jenna Vickery for the use and training of their Nikon Eclipse Ti2 inverted light microscope, and Christine Childs, Kristina Terrell and Dmitry Baturin of the University of Colorado Cancer Center Flow Cytometry Shared Resource for training and assistance with flow cytometry. We thank Dr. Laurie Krug and Dr. Craig Forrest for generously sharing the ORF59.GFP recombinant virus. R.E.K. was supported by the Molecular Biology T32 pre-doctoral training grant (NIH 5T32GM136444). C.G. was supported by the University of Colorado School of Medicine RNA Bioscience Initiative Summer Internship Program. This study was supported by National Institutes of Health grant R01 AI157201 awarded to LvD and ETC, with additional support by the National Institutes of Health Cancer Center Support Grant (P30CA046934), including assistance from the Bioinformatics and Biostatistics Shared Resource (RRID: SCR_021983), Flow Cytometry Shared Resource (RRID: SCR_022035), and Genomics Shared Resource (RRID: SCR_021984). Generative AI was not used in preparation of this manuscript.

Contributor Roles

Conceptualization: G.V., E.T.C., L.F.v.D.

Methodology: D.G.O.

Validation: G.V., K.S.N., A.T., R.E.K., E.A.A., S.C., C.G., M.D., B.D.G.

Formal analysis: A.G., E.T.C.

Investigation: G.V., K.S.N., A.T., R.E.K., E.A.A., S.C., C.G., M.D., B.D.G., E.M.M.

Data curation: G.V., A.G., E.T.C.

Writing – original draft: G.V., E.T.C., L.F.v.D.

Writing – review & editing: G.V., E.T.C., L.F.v.D.

Visualization: G.V., A.G., E.T.C., L.F.v.D.

Supervision: E.T.C., L.F.v.D.

Project administration: G.V., E.T.C., L.F.v.D.

Funding acquisition: E.T.C., L.F.v.D.

References:

1. Longnecker, R. and F. Neipel, *Introduction to the human gamma-herpesviruses*, in *Human Herpesviruses: Biology, Therapy, and Immunoprophylaxis*, A. Arvin, et al., Editors. 2007: Cambridge.
2. Mariggio, G., S. Koch, and T.F. Schulz, *Kaposi sarcoma herpesvirus pathogenesis.* Philos Trans R Soc Lond B Biol Sci, 2017. **372**(1732).
3. Young, L.S., L.F. Yap, and P.G. Murray, *Epstein-Barr virus: more than 50 years old and still providing surprises.* Nat Rev Cancer, 2016. **16**(12): p. 789-802.
4. Virgin, H.W.t., et al., *Complete sequence and genomic analysis of murine gammaherpesvirus 68.* J Virol, 1997. **71**(8): p. 5894-904.
5. Wang, Y., S.A. Tibbetts, and L.T. Krug, *Conquering the Host: Determinants of Pathogenesis Learned from Murine Gammaherpesvirus 68.* Annu Rev Virol, 2021. **8**(1): p. 349-371.
6. Oko, L.M., et al., *Multidimensional analysis of Gammaherpesvirus RNA expression reveals unexpected heterogeneity of gene expression.* PLoS Pathog, 2019. **15**(6): p. e1007849.
7. Landis, J.T., et al., *Evidence for Multiple Subpopulations of Herpesvirus-Latently Infected Cells.* mBio, 2022: p. e0347321.
8. Jung, K.L., et al., *Single-cell analysis of Kaposi's sarcoma-associated herpesvirus infection in three-dimensional air-liquid interface culture model.* PLoS Pathog, 2022. **18**(8): p. e1010775.
9. Berger, J.N., et al., *Redefining De Novo Gammaherpesvirus Infection Through High-Dimensional, Single-Cell Analysis of Virus and Host.* bioRxiv, 2020.
10. SoRelle, E.D., et al., *Epstein-Barr virus reactivation induces divergent abortive, reprogrammed, and host shutoff states by lytic progression.* PLoS Pathog, 2024. **20**(10): p. e1012341.
11. Salek-Ardakani, S., S.A. Lyons, and J.R. Arrand, *Epstein-Barr virus promotes human monocyte survival and maturation through a paracrine induction of IFN-alpha.* J Immunol, 2004. **173**(1): p. 321-31.
12. Tugizov, S., et al., *Epstein-Barr virus (EBV)-infected monocytes facilitate dissemination of EBV within the oral mucosal epithelium.* J Virol, 2007. **81**(11): p. 5484-96.
13. Torii, Y., et al., *Epstein-Barr virus infection-induced inflammasome activation in human monocytes.* PLoS One, 2017. **12**(4): p. e0175053.
14. Frederico, B., et al., *Myeloid infection links epithelial and B cell tropisms of Murid Herpesvirus-4.* PLoS Pathog, 2012. **8**(9): p. e1002935.
15. Weck, K.E., et al., *Macrophages are the major reservoir of latent murine gammaherpesvirus 68 in peritoneal cells.* J Virol, 1999. **73**(4): p. 3273-83.
16. West, J. and B. Damania, *Upregulation of the TLR3 pathway by Kaposi's sarcoma-associated herpesvirus during primary infection.* J Virol, 2008. **82**(11): p. 5440-9.
17. Gregory, S.M., et al., *Discovery of a viral NLR homolog that inhibits the inflammasome.* Science, 2011. **331**(6015): p. 330-4.
18. Gregory, S.M., et al., *Latent Kaposi's sarcoma-associated herpesvirus infection of monocytes downregulates expression of adaptive immune response costimulatory receptors and proinflammatory cytokines.* J Virol, 2012. **86**(7): p. 3916-23.
19. Host, K.M., et al., *Kaposi's Sarcoma-Associated Herpesvirus Increases PD-L1 and Proinflammatory Cytokine Expression in Human Monocytes.* mBio, 2017. **8**(5).
20. Kerur, N., et al., *Characterization of entry and infection of monocytic THP-1 cells by Kaposi's sarcoma associated herpesvirus (KSHV): role of heparan sulfate, DC-SIGN, integrins and signaling.* Virology, 2010. **406**(1): p. 103-16.
21. Savard, M., et al., *Infection of primary human monocytes by Epstein-Barr virus.* J Virol, 2000. **74**(6): p. 2612-9.

785 22. Shimoda, M., et al., *Virally encoded interleukin-6 facilitates KSHV replication in*
786 *monocytes and induction of dysfunctional macrophages.* PLoS Pathog, 2023. **19**(10): p.
787 e1011703.
788 23. Li, H., et al., *A replication-defective gammaherpesvirus efficiently establishes long-term*
789 *latency in macrophages but not in B cells in vivo.* J Virol, 2008. **82**(17): p. 8500-8.
790 24. Tarakanova, V.L., et al., *Gamma-herpesvirus kinase actively initiates a DNA damage*
791 *response by inducing phosphorylation of H2AX to foster viral replication.* Cell Host
792 Microbe, 2007. **1**(4): p. 275-86.
793 25. Tarakanova, V.L., et al., *MHV68 complement regulatory protein facilitates MHV68*
794 *replication in primary macrophages in a complement independent manner.* Virology,
795 2010. **396**(2): p. 323-8.
796 26. Szymula, A., et al., *Macrophages drive KSHV B cell latency.* Cell Rep, 2023. **42**(7): p.
797 112767.
798 27. Gaspar, M., et al., *Murid herpesvirus-4 exploits dendritic cells to infect B cells.* PLoS
799 Pathog, 2011. **7**(11): p. e1002346.
800 28. Lange, P.T., M.C. White, and B. Damania, *Activation and Evasion of Innate Immunity by*
801 *Gammaherpesviruses.* J Mol Biol, 2022. **434**(6): p. 167214.
802 29. Bussey, K.A., et al., *The gammaherpesviruses Kaposi's sarcoma-associated herpesvirus*
803 *and murine gammaherpesvirus 68 modulate the Toll-like receptor-induced*
804 *proinflammatory cytokine response.* J Virol, 2014. **88**(16): p. 9245-59.
805 30. Rosa, G.T., et al., *IgG fc receptors provide an alternative infection route for murine*
806 *gamma-herpesvirus-68.* PLoS One, 2007. **2**(6): p. e560.
807 31. Lawler, C., et al., *Rhadinovirus host entry by co-operative infection.* PLoS Pathog, 2015.
808 **11**(3): p. e1004761.
809 32. Flano, E., et al., *Latent murine gamma-herpesvirus infection is established in activated B*
810 *cells, dendritic cells, and macrophages.* J Immunol, 2000. **165**(2): p. 1074-81.
811 33. Frederico, B., et al., *A murid gamma-herpesviruses exploits normal splenic immune*
812 *communication routes for systemic spread.* Cell Host Microbe, 2014. **15**(4): p. 457-70.
813 34. Frederico, B., et al., *Subcapsular sinus macrophages limit acute gammaherpesvirus*
814 *dissemination.* J Gen Virol, 2015. **96**(8): p. 2314-2327.
815 35. Lange, P.T., et al., *Liver X Receptors Suppress Activity of Cholesterol and Fatty Acid*
816 *Synthesis Pathways To Oppose Gammaherpesvirus Replication.* mBio, 2018. **9**(4).
817 36. Aurubin, C.A., et al., *Low-Density Lipoprotein Receptor Suppresses the Endogenous*
818 *Cholesterol Synthesis Pathway To Oppose Gammaherpesvirus Replication in Primary*
819 *Macrophages.* J Virol, 2021. **95**(17): p. e0064921.
820 37. Reese, T.A., et al., *Helminth infection reactivates latent gamma-herpesvirus via cytokine*
821 *competition at a viral promoter.* Science, 2014. **345**(6196): p. 573-7.
822 38. Mounce, B.C., et al., *Gammaherpesvirus gene expression and DNA synthesis are*
823 *facilitated by viral protein kinase and histone variant H2AX.* Virology, 2011. **420**(2): p.
824 73-81.
825 39. Ramaswami, R., et al., *Transcriptional landscape of Kaposi sarcoma tumors identifies*
826 *unique immunologic signatures and key determinants of angiogenesis.* J Transl Med,
827 2023. **21**(1): p. 653.
828 40. Nair, A., et al., *The elevated expression of ORF75, a KSHV lytic gene, in Kaposi*
829 *sarcoma lesions is driven by a GC-rich DNA cis element in its promoter region.* PLoS
830 Pathog, 2025. **21**(3): p. e1012984.
831 41. Abbott, R.J., et al., *CD8+ T cell responses to lytic EBV infection: late antigen specificities*
832 *as subdominant components of the total response.* J Immunol, 2013. **191**(11): p. 5398-
833 409.
834 42. Sagou, K., et al., *Epstein-Barr virus lytic gene BNRF1 promotes B-cell lymphomagenesis*
835 *via IFI27 upregulation.* PLoS Pathog, 2024. **20**(2): p. e1011954.

836 43. Nealy, M.S., et al., *Use of a virus-encoded enzymatic marker reveals that a stable*
837 *fraction of memory B cells expresses latency-associated nuclear antigen throughout*
838 *chronic gammaherpesvirus infection.* J Virol, 2010. **84**(15): p. 7523-34.
839 44. Diebel, K.W., et al., *Gammaherpesvirus small noncoding RNAs are bifunctional*
840 *elements that regulate infection and contribute to virulence in vivo.* mBio, 2015. **6**(1): p.
841 e01670-14.
842 45. Kulkarni, A., et al., *Beyond bulk: a review of single cell transcriptomics methodologies*
843 *and applications.* Curr Opin Biotechnol, 2019. **58**: p. 129-136.
844 46. Van Skike, N.D., et al., *Viral FGARAT ORF75A promotes early events in lytic infection*
845 *and gammaherpesvirus pathogenesis in mice.* PLoS Pathog, 2018. **14**(2): p. e1006843.
846 47. Zhang, Z., et al., *A greedy algorithm for aligning DNA sequences.* J Comput Biol, 2000.
847 **7**(1-2): p. 203-14.
848 48. Weck, K.E., et al., *Mature B cells are required for acute splenic infection, but not for*
849 *establishment of latency, by murine gammaherpesvirus 68.* J Virol, 1996. **70**(10): p.
850 6775-80.
851 49. Cheng, B.Y., et al., *Tiled microarray identification of novel viral transcript structures and*
852 *distinct transcriptional profiles during two modes of productive murine*
853 *gammaherpesvirus 68 infection.* J Virol, 2012. **86**(8): p. 4340-57.
854 50. Forrest, J.C. and S.H. Speck, *Establishment of B-cell lines latently infected with*
855 *reactivation-competent murine gammaherpesvirus 68 provides evidence for viral*
856 *alteration of a DNA damage-signaling cascade.* J Virol, 2008. **82**(15): p. 7688-99.
857 51. Smith, K.R., et al., *Uracil-DNA glycosylase of murine gammaherpesvirus 68 binds*
858 *cognate viral replication factors independently of its catalytic residues.* mSphere, 2023.
859 **8**(5): p. e0027823.
860 52. Bieniasz, P.D., *Intrinsic immunity: a front-line defense against viral attack.* Nat Immunol,
861 2004. **5**(11): p. 1109-15.
862 53. Yan, N. and Z.J. Chen, *Intrinsic antiviral immunity.* Nat Immunol, 2012. **13**(3): p. 214-22.
863 54. Covarrubias, S., et al., *Host shutoff is a conserved phenotype of gammaherpesvirus*
864 *infection and is orchestrated exclusively from the cytoplasm.* J Virol, 2009. **83**(18): p.
865 9554-66.
866 55. Wang, G., et al., *Th2 Cytokine Modulates Herpesvirus Reactivation in a Cell Type*
867 *Specific Manner.* J Virol, 2021.
868 56. van Dyk, L.F., H.W.t. Virgin, and S.H. Speck, *The murine gammaherpesvirus 68 v-cyclin*
869 *is a critical regulator of reactivation from latency.* J Virol, 2000. **74**(16): p. 7451-61.
870 57. Wu, T.T., et al., *Rta of murine gammaherpesvirus 68 reactivates the complete lytic cycle*
871 *from latency.* J Virol, 2000. **74**(8): p. 3659-67.
872 58. Pavlova, I.V., H.W.t. Virgin, and S.H. Speck, *Disruption of gammaherpesvirus 68 gene*
873 *50 demonstrates that Rta is essential for virus replication.* J Virol, 2003. **77**(10): p. 5731-
874 9.
875 59. Wu, T.T., et al., *Function of Rta is essential for lytic replication of murine*
876 *gammaherpesvirus 68.* J Virol, 2001. **75**(19): p. 9262-73.
877 60. Martinez-Guzman, D., et al., *Transcription program of murine gammaherpesvirus 68.* J
878 Virol, 2003. **77**(19): p. 10488-503.
879 61. Gunther, T., et al., *A comparative epigenome analysis of gammaherpesviruses suggests*
880 *cis-acting sequence features as critical mediators of rapid polycomb recruitment.* PLoS
881 Pathog, 2019. **15**(10): p. e1007838.
882 62. Coleman, H.M., S. Efstathiou, and P.G. Stevenson, *Transcription of the murine*
883 *gammaherpesvirus 68 ORF73 from promoters in the viral terminal repeats.* J Gen Virol,
884 2005. **86**(Pt 3): p. 561-574.

885 63. Rose, T.M., et al., *Quantitative RNAseq analysis of Ugandan KS tumors reveals KSHV*
886 *gene expression dominated by transcription from the LTd downstream latency promoter.*
887 PLoS Pathog, 2018. **14**(12): p. e1007441.
888 64. Ramaswami, R., et al., *Transcriptional analysis identifies overlapping and tissue-distinct*
889 *profiles between Kaposi sarcoma tumors of the skin and gastrointestinal tract.* bioRxiv,
890 2022: p. 2022.03.18.484923.
891 65. Freeman, M.L., et al., *CD4 T cells specific for a latency-associated gamma-herpesvirus*
892 *epitope are polyfunctional and cytotoxic.* J Immunol, 2014. **193**(12): p. 5827-34.
893 66. Gredmark-Russ, S., et al., *The CD8 T-cell response against murine gammaherpesvirus*
894 *68 is directed toward a broad repertoire of epitopes from both early and late antigens.* J
895 Virol, 2008. **82**(24): p. 12205-12.
896 67. Freeman, M.L., et al., *Two kinetic patterns of epitope-specific CD8 T-cell responses*
897 *following murine gammaherpesvirus 68 infection.* J Virol, 2010. **84**(6): p. 2881-92.
898 68. Tan, C.S.E., C. Lawler, and P.G. Stevenson, *CD8+ T cell evasion mandates CD4+ T cell*
899 *control of chronic gamma-herpesvirus infection.* PLoS Pathog, 2017. **13**(4): p. e1006311.
900 69. Darrah, E.J., et al., *ATM supports gammaherpesvirus replication by attenuating type I*
901 *interferon pathway.* Virology, 2017. **510**: p. 137-146.
902 70. Schmalzriedt, D.L., et al., *Apolipoprotein E selectively supports gammaherpesvirus*
903 *replication in macrophages.* J Virol, 2025. **99**(6): p. e0048025.
904 71. Riggs, J.B., et al., *Optimized Detection of Acute MHV68 Infection With a Reporter*
905 *System Identifies Large Peritoneal Macrophages as a Dominant Target of Primary*
906 *Infection.* Front Microbiol, 2021. **12**: p. 656979.
907 72. Zarek, C.M., et al., *Preexisting helminth challenge exacerbates infection and reactivation*
908 *of gammaherpesvirus in tissue resident macrophages.* PLoS Pathog, 2023. **19**(10): p.
909 e1011691.
910 73. Goodwin, M.M., et al., *Murine gammaherpesvirus 68 has evolved gamma interferon and*
911 *stat1-repressible promoters for the lytic switch gene 50.* J Virol, 2010. **84**(7): p. 3711-7.
912 74. Mboko, W.P., et al., *Interferon Regulatory Factor 1 and Type I Interferon Cooperate To*
913 *Control Acute Gammaherpesvirus Infection.* J Virol, 2017. **91**(1).
914 75. Mounce, B.C., et al., *A conserved gammaherpesvirus protein kinase targets histone*
915 *deacetylases 1 and 2 to facilitate viral replication in primary macrophages.* J Virol, 2013.
916 **87**(13): p. 7314-25.
917 76. Steed, A., et al., *Gamma interferon blocks gammaherpesvirus reactivation from latency*
918 *in a cell type-specific manner.* J Virol, 2007. **81**(11): p. 6134-40.
919 77. Rickabaugh, T.M., et al., *Generation of a latency-deficient gammaherpesvirus that is*
920 *protective against secondary infection.* J Virol, 2004. **78**(17): p. 9215-23.
921 78. Pfaffl, M.W., *A new mathematical model for relative quantification in real-time RT-PCR.*
922 Nucleic Acids Res, 2001. **29**(9): p. e45.
923 79. Coomes, S.M., et al., *Severe gammaherpesvirus-induced pneumonitis and fibrosis in*
924 *syngeneic bone marrow transplant mice is related to effects of transforming growth*
925 *factor-beta.* Am J Pathol, 2011. **179**(5): p. 2382-96.
926 80. Knox, A.N., et al., *Lytic Infection with Murine Gammaherpesvirus 68 Activates Host and*
927 *Viral RNA Polymerase III Promoters and Enhances Noncoding RNA Expression.* J Virol,
928 2021. **95**(14): p. e0007921.
929 81. Zheng, G.X., et al., *Massively parallel digital transcriptional profiling of single cells.* Nat
930 Commun, 2017. **8**: p. 14049.
931 82. Hao, Y., et al., *Integrated analysis of multimodal single-cell data.* Cell, 2021. **184**(13): p.
932 3573-3587 e29.
933 83. Wickham, H., *ggplot2: Elegant Graphics for Data Analysis*. 2016: Springer-Verlag New
934 York.

935 84. Kapadia, S.B., et al., *Murine gammaherpesvirus 68 encodes a functional regulator of*
936 *complement activation.* J Virol, 1999. **73**(9): p. 7658-70.
937

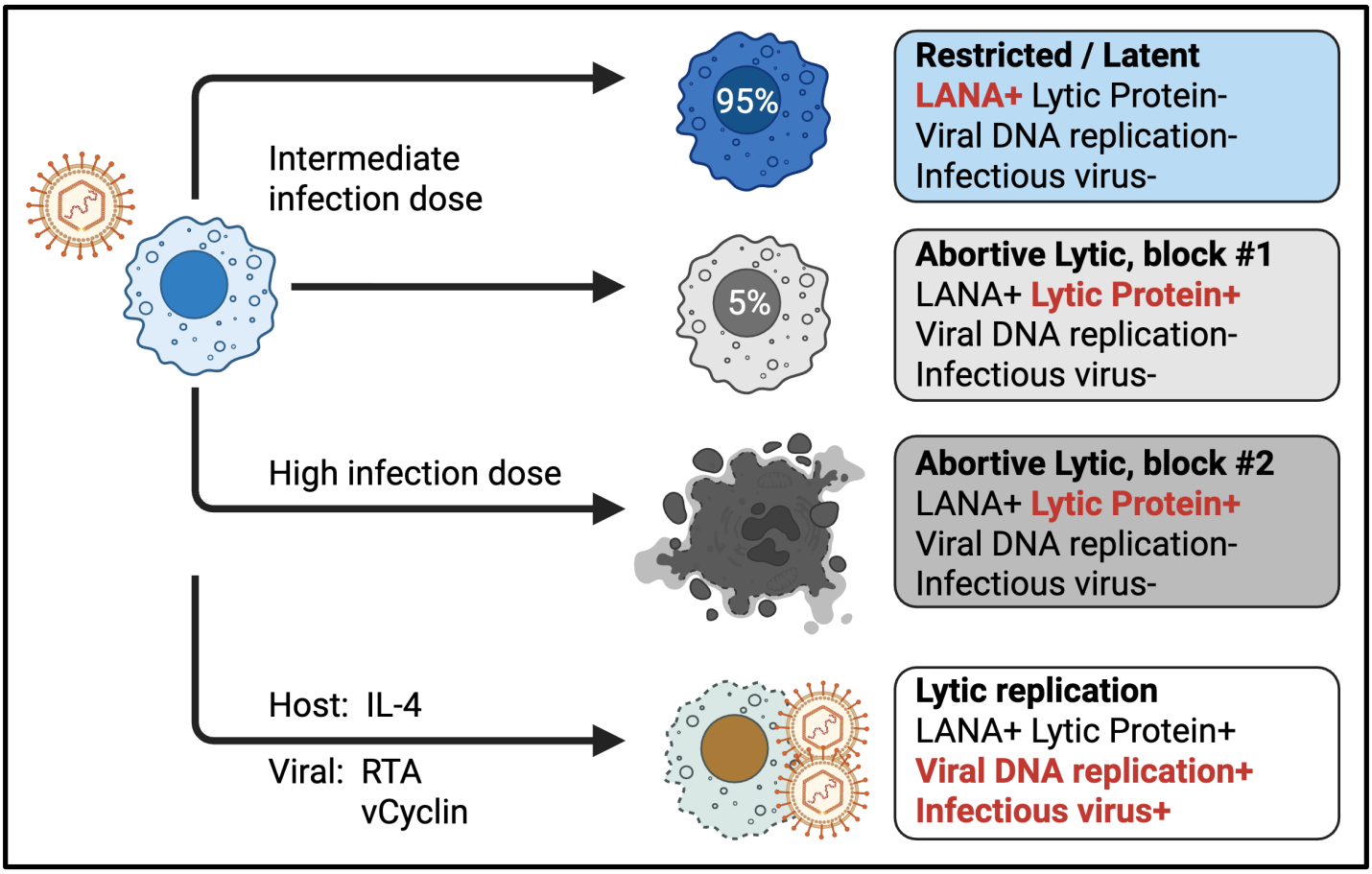

Highlights

- MHV68 efficiently infects macrophages
- Infection results in three divergent outcomes regulated by discrete inputs
- Macrophages limit lytic replication at two distinct stages
- Macrophages are capable of lytic replication, promoted by the host cytokine IL-4 and viral genes.

Vragel et al
Graphic Abstract
Highlights

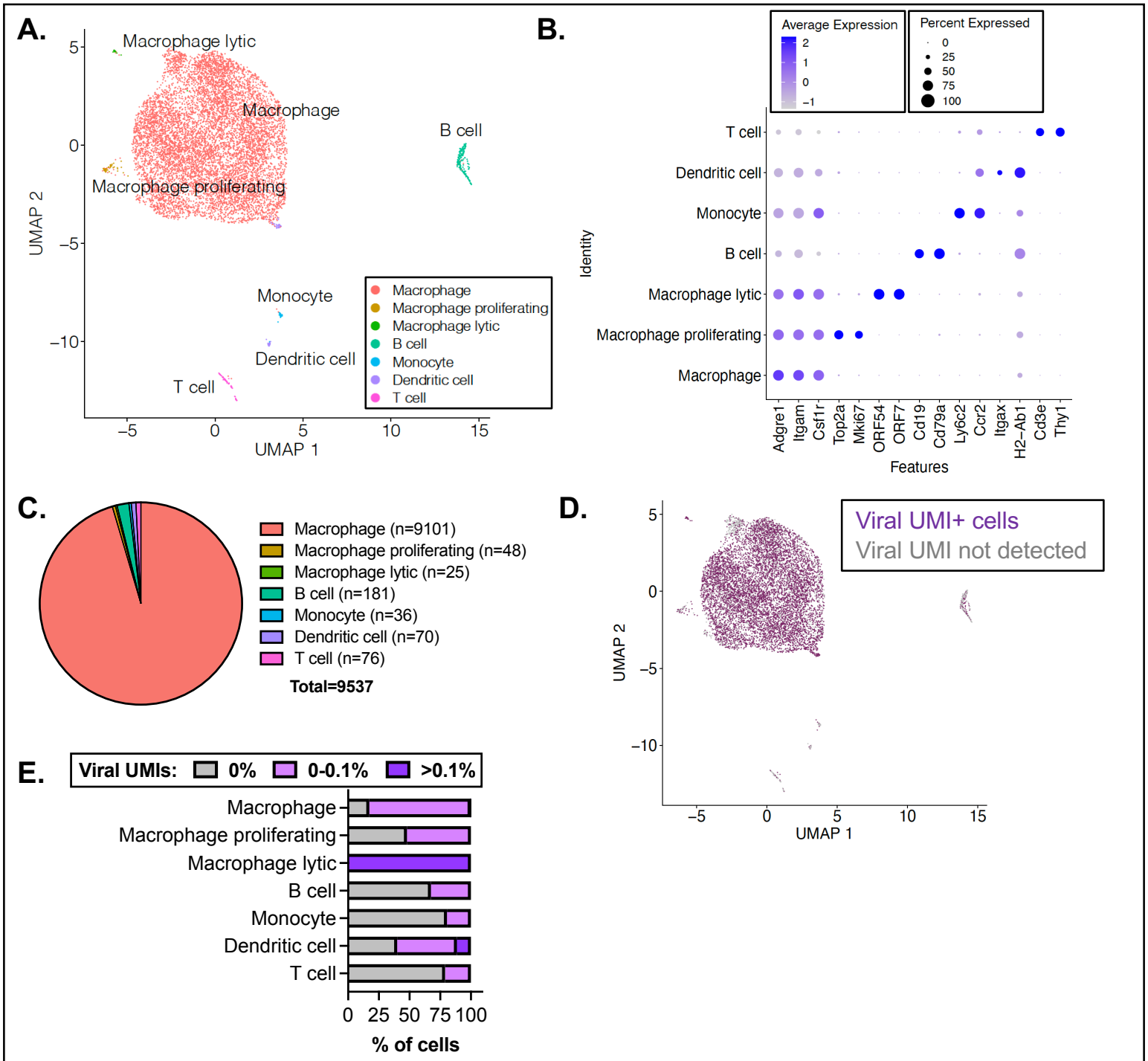

Vragel et al
Fig. 1

Figure 1. Single cell RNA sequencing analysis of acute MHV68 macrophage infection. C57BL/6J mice were infected with $1x10^6$ PFU of WT MHV68.LANAβlac virus, with MHV68-infected, LANAβlac+ peritoneal cells sort-purified at 16 hpi and subjected to scRNA-seq analysis. **(A-B)** Visualization of cell types based on lineage marker genes depicted in panel B. **(C)** Quantification of cell subsets defined by scRNA-seq. **(D)** UMAP visualization of cells with at least 1 viral UMI detected per cell identified by purple. **(E)** Frequency of cells stratified by the fraction of viral UMIs out of total UMIs detected per cell. 56 cells had >0.1% of total UMIs contributed by viral UMIs, including 23 of 9101 macrophages (0.25%), 25 of 25 macrophages with lytic gene expression (100%) and 8 of 70 dendritic cells (11.43%). Data are from 9,537 cells, with cell subsets enumerated in panel C. Supporting data in **Fig S1-S2**.

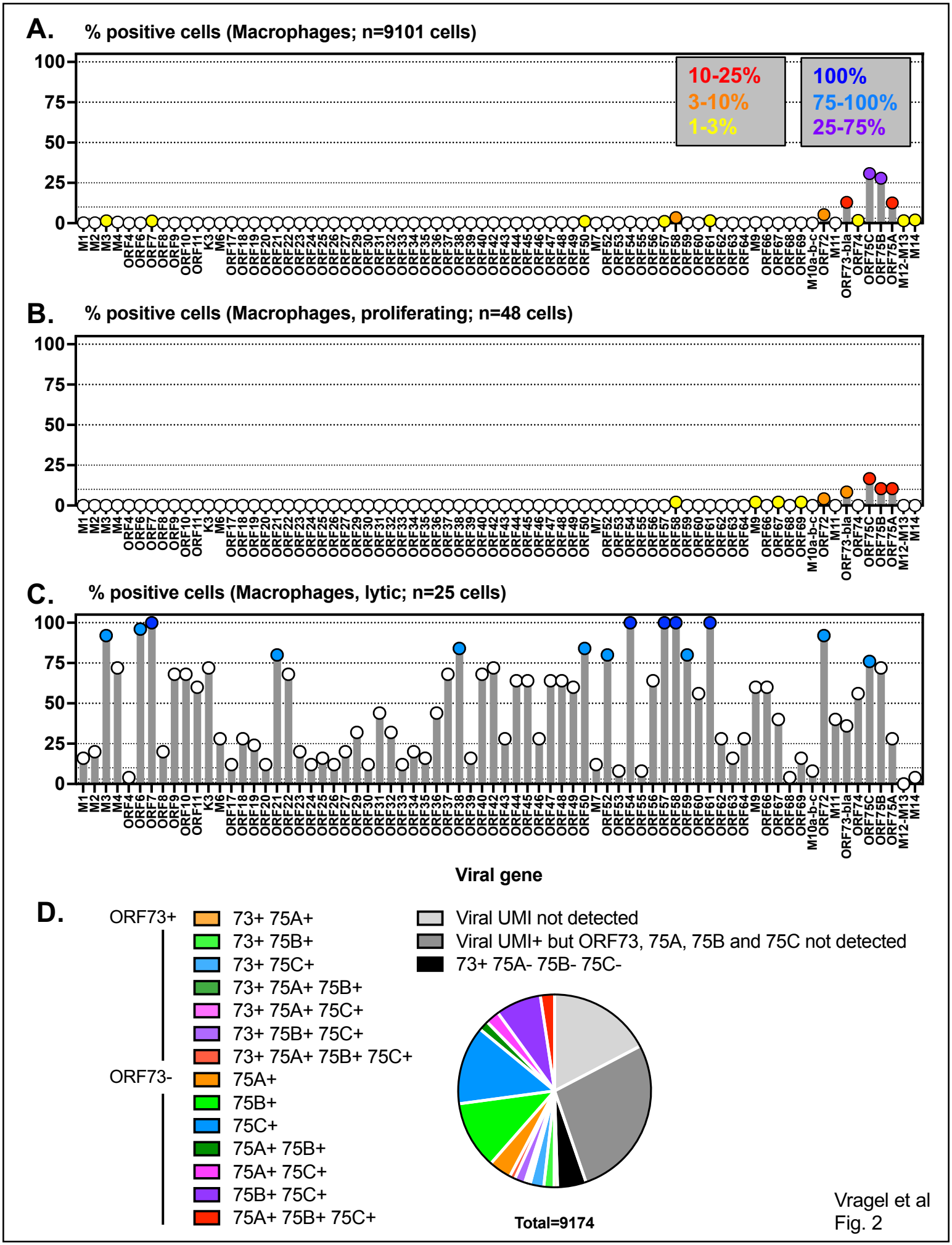

Vragel et al
Fig. 2

Figure 2. Single cell RNA sequencing analysis of acute MHV68 macrophage infection reveals two distinct transcriptional profiles. Analysis of viral gene expression defined by scRNA-seq in macrophage subsets from **Figure 1. (A-C)** Frequency of cells with detectable reads mapping to MHV68 genes, comparing (A) macrophages (82.79% viral UMI+), (B) macrophages with proliferative gene signature (52.08% viral UMI+), or (C) macrophages with lytic gene expression (100% viral UMI+). Viral genes are indicated on the x axis, arranged from left to right based on the published MHV68 genome, with the frequency of cells positive for each viral gene depicted on the y axis. To facilitate comparison of gene expression across the viral genome and cell populations, circles are color-coded to identify values that are in the indicated ranges (defined in key, panel A). Dotted lines indicate different thresholds for viral gene positivity, empirically defined. For panel C, only genes with >75% positivity were color-coded, given the limited number of cells. **(D)** Frequency among macrophages defined by detection of ORF73, ORF75A, ORF75B, and ORF75C RNAs, enumerating all potential gene combinations macrophages from panels A-C.

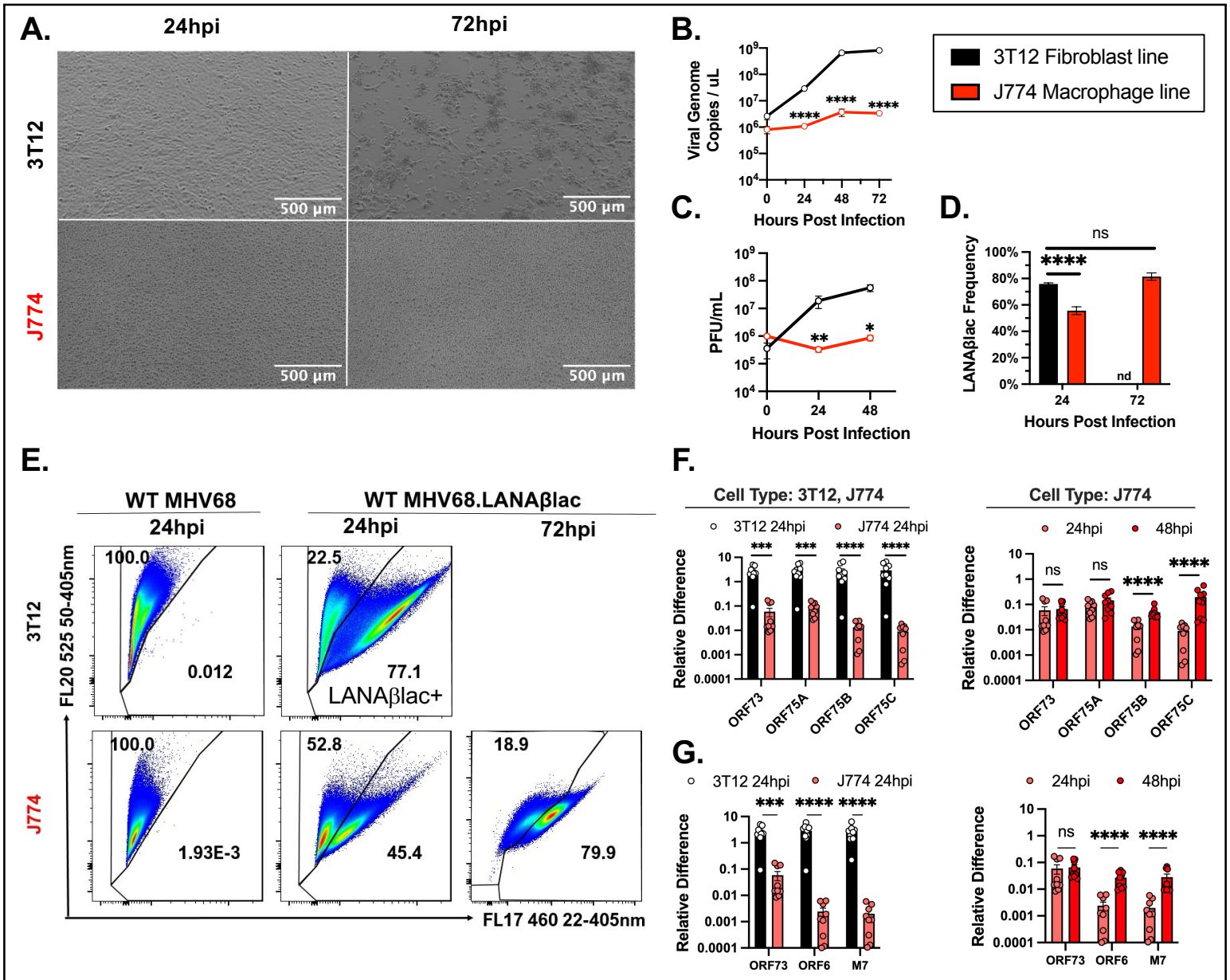

Vragel et al
Fig. 3

Figure 3. MHV68 readily infects J774 macrophages with limited lytic transcription. Analysis of MHV68 infection (WT MHV68.LANAβlac, MOI=1 PFU/cell) comparing 3T12 fibroblasts and J774 macrophages. **(A)** Representative brightfield images of infected 3T12 (top) or J774 cells (bottom) early (24 hpi, left) or late (72 hpi, right) post-infection. 3T12 cells showed cytopathic effect (CPE), including cell rounding (24 hpi) and monolayer destruction (72 hpi), in contrast to J774 cells. **(B)** Viral DNA quantitation defined by qPCR. **(C)** Virus replication defined by plaque assay. **(D-E)** Frequency of MHV68-infected, LANAβlac+ cells defined by flow cytometry, detected by CCF2 substrate cleavage, analyzing single, viable cells. Samples infected with WT MHV68 (left, panel E) define background signal and do not encode LANAβlac. **(F-G)** Quantitation of viral gene expression defined by qRT-PCR, comparing 3T12 and J774 cells at 24 hpi (left) or J774 cells at 24 and 48 hpi (right). Flow cytometric analysis focused on single, viable cells. Data depict mean ± SEM, from 3 independent experiments with 3 biological replicates per experiment (B, D, F-G) or 2 (t=0) or 6 (t=24, 48 hpi) independent experiments (C), with individual symbols representing independent biological samples. Statistical analysis was done using unpaired t test, with statistically significant differences indicated, *$p<0.05$, **$p<0.01$, ***$p<0.001$, ****$p<0.0001$.

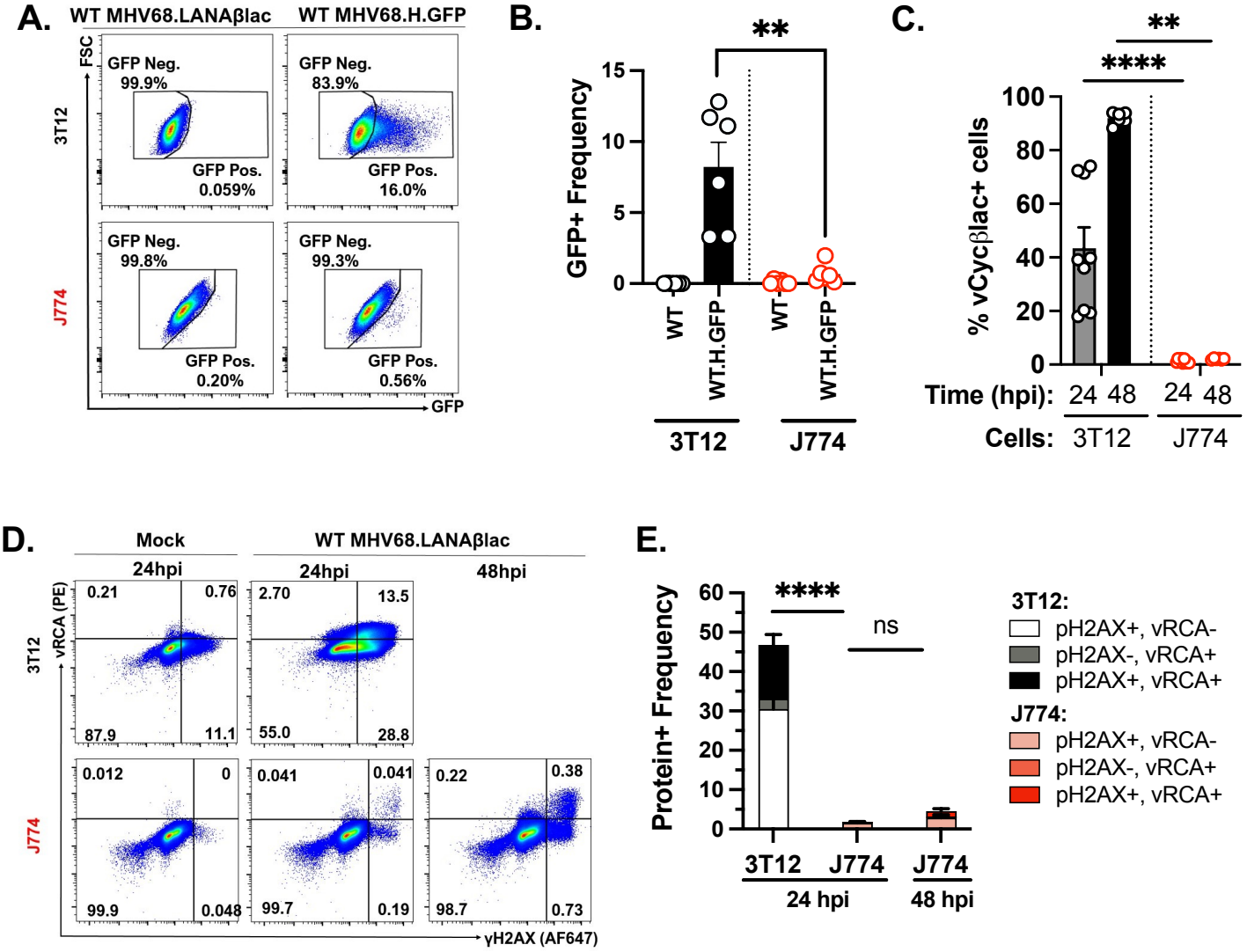

Vragel et al
Fig. 4

Figure 4. Only rare MHV68 infected macrophages display lytic gene expression. Analysis of MHV68 infection and lytic cycle profiles with either MHV68.H.GFP or MHV68.LANAβlac (MOI=1 PFU/cell) comparing 3T12 fibroblasts and J774 macrophages. **(A)** Flow cytometric analysis of virus-expressed GFP in 3T12 or J774 cells 18 hpi. Data depict the frequency of cells with GFP expression, an indicator of MHV68.H.GFP infection. Background fluorescence defined by WT MHV68.LANAβlac-infected cells (left column), without the addition of the CCF2 fluorescent substrate. **(B)** Frequency of HygroGFP+ cells defined by flow cytometry, as in panel A. **(C)** Frequency of vCycβlac+ cells defined by flow cytometry. **(D)** Flow cytometric analysis of lytic infection-associated proteins, vRCA and γH2AX in 3T12 (top) or J774 (bottom) cells, comparing mock (left) or WT MHV68.LANAβlac-infected cells. Data for 3T12 cells at 48 hpi was not assessed due to extensive cell destruction. **(E)** Quantification of the frequency of infected cells with protein expression associated with lytic infection defined by flow cytometry, as in panel D. Flow cytometry data focus on single, viable cells defined using gating strategies in **Supp. Fig. S3A** and **S4B**. Data show mean ± SEM from 3 experiments, with 2 (B,E) or 3 samples (C) per experiment. Statistical analysis done using Mann-Whitney test, with statistically significant differences as indicated, **$p<0.01$, ****$p<0.0001$.

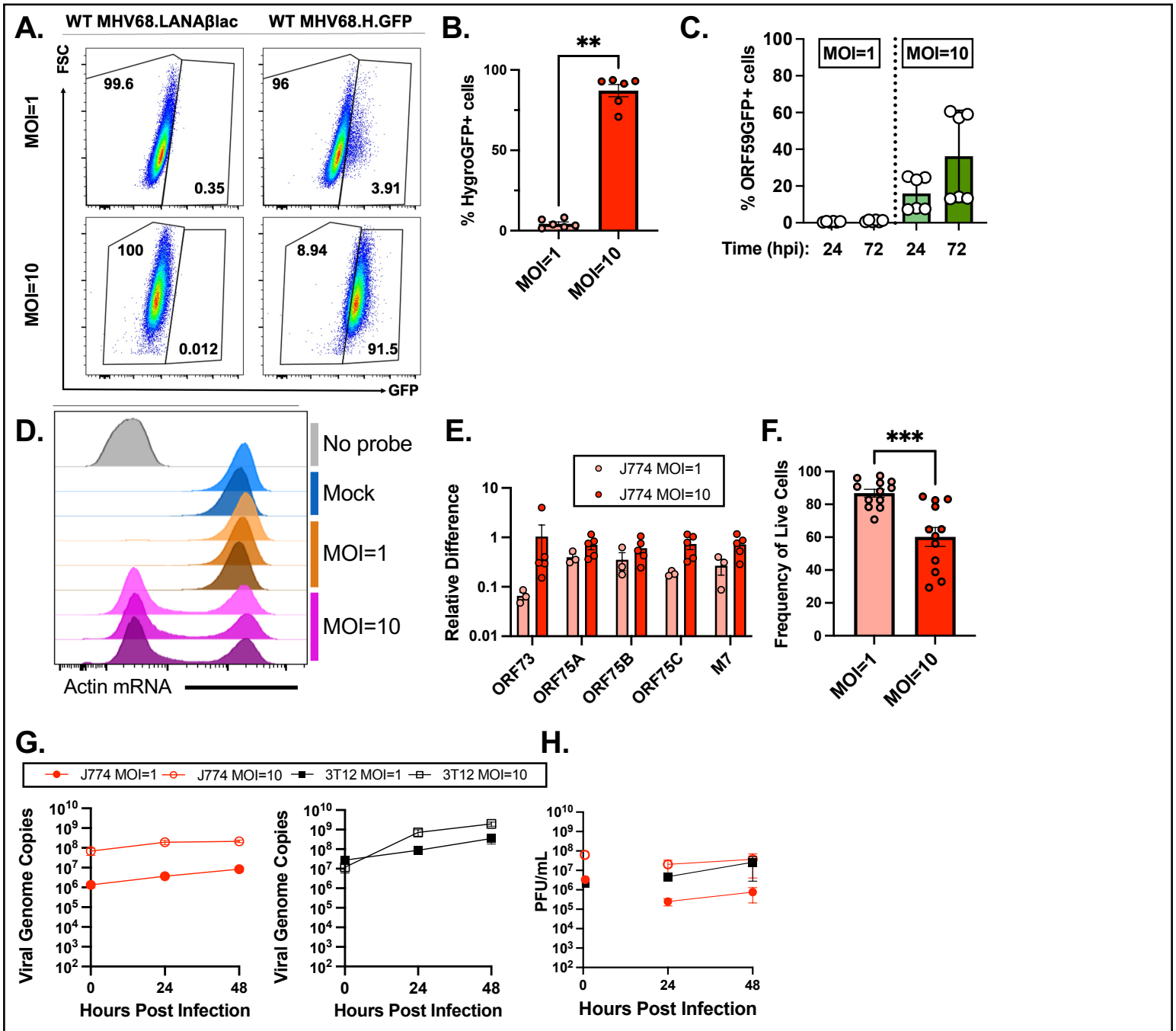

Vragel et al
Fig. 5

Figure 5. High dose MHV68 infection results in abortive replication. MHV68 outcomes in J774 macrophages comparing intermediate (MOI=1 PFU/cell) or high dose (MOI=10) infection. **(A)** Flow cytometric analysis of GFP in MHV68.LANAβlac- (left; negative control with no CCF2 substrate) or MHV68.H.GFP-infected cells (right) at MOI=1 (top) or MOI=10 (bottom). **(B)** Frequency of GFP+ cells quantified by flow cytometry, as in A. **(C)** Frequency of ORF59GFP+ J774 cells quantified by flow cytometry at 24 or 72 hpi. **(D)** Flow cytometric analysis of actin mRNA levels 24 hpi in mock or WT MHV68-infected cells with individual rows showing independent biological samples. **(E)** Quantitation of viral RNA expression by qRT-PCR standardized to 18S RNA, comparing intermediate or high MOI (MHV68.LANAβlac) at the indicated timepoints. **(F)** Frequency of MHV68.HygroGFP-infected single cells that are viable, quantified by flow cytometry. **(G)** Quantitation of viral DNA by qPCR in J774 (left) or 3T12 cells (right) as a function of MOI (MHV68.LANAβlac). **(H)** Infectious virus production quantified by plaque assay, comparing 3T12 cells (MOI=1) with J774 cells (MOI=1 or 10). Flow cytometry data analyzed single, viable cells (A-D) or single cells (F), with gating strategy in **Supp. Fig. 3**. Data show mean ± SEM, with individual symbols showing independent biological samples from 2-3 independent experiments with 2-3 biological replicates per experiment. Statistical analysis was done using Mann-Whitney test with statistically significant differences indicated, **$p<0.01$, ***$p<0.001$.

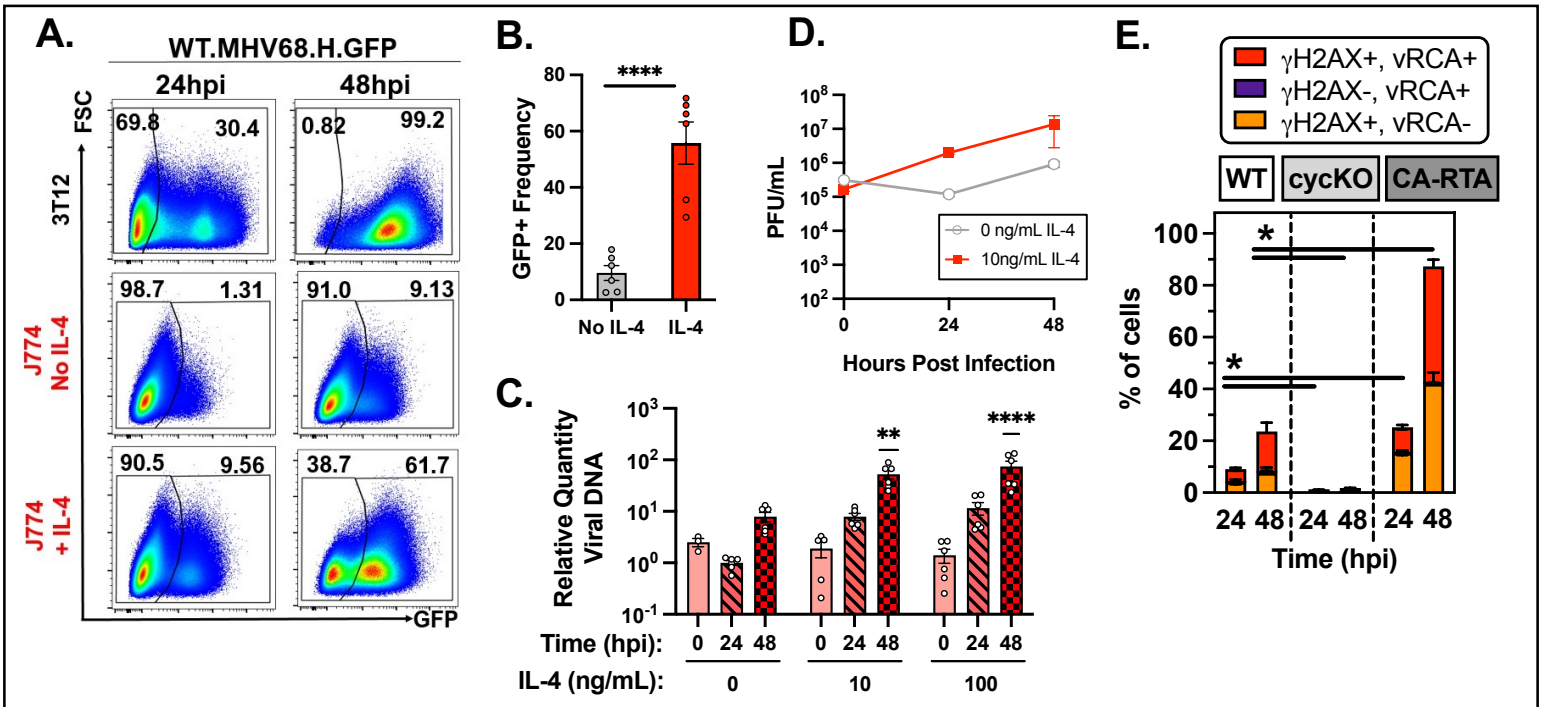

Vragel et al
Fig. 6

Figure 6. MHV68 infection of macrophages is modulated by host and viral factors. All infections done with MOI=1. **(A-D)** IL-4 effect on MHV68 infection and genome replication in J774 macrophages. IL-4 cultures were pretreated with IL-4 for 16-18 hours at the indicated concentration, with fresh IL-4 replenished after infection. **(A)** Flow cytometric analysis of MHV68.H.GFP infection in 3T12 (top), untreated J774 (middle) or IL4-treated J774 cells at 24 (left) or 48 hpi (right), analyzing single, viable cells. **(B)** Frequency of GFP+ cells quantified by flow cytometry, as in A. **(C-D)** IL-4 effect on viral DNA replication **(C)** and infectious virus production **(D)** in WT MHV68-infected J774 cells. **(E)** Frequency of J774 cells expressing markers of lytic infection (γH2AX, vRCA) quantified by flow cytometry, comparing WT, vCycKO or CA-RTA MHV68 at 24 or 48 hpi. Flow cytometric analysis focused on single, viable cells. Data depict mean ± SEM, with individual symbols representing independent biological samples from 2-3 independent experiments with 2-3 biological replicates per experiment (B,C,E) or from 1-2 independent experiments with 3 biological replicates measured (D). Statistical analysis used (B) unpaired t test, (C) one-way ANOVA comparing samples collected at the same timepoint untreated versus cytokine treated, or (E) one-way ANOVA comparing samples collected at the same timepoint with WT infection (nonparametric Kruskal-Willis test subjected to Dunn's multiple comparison test), with statistically significant differences indicated, *$p<0.05$, **$p<0.01$, ****$p<0.0001$.

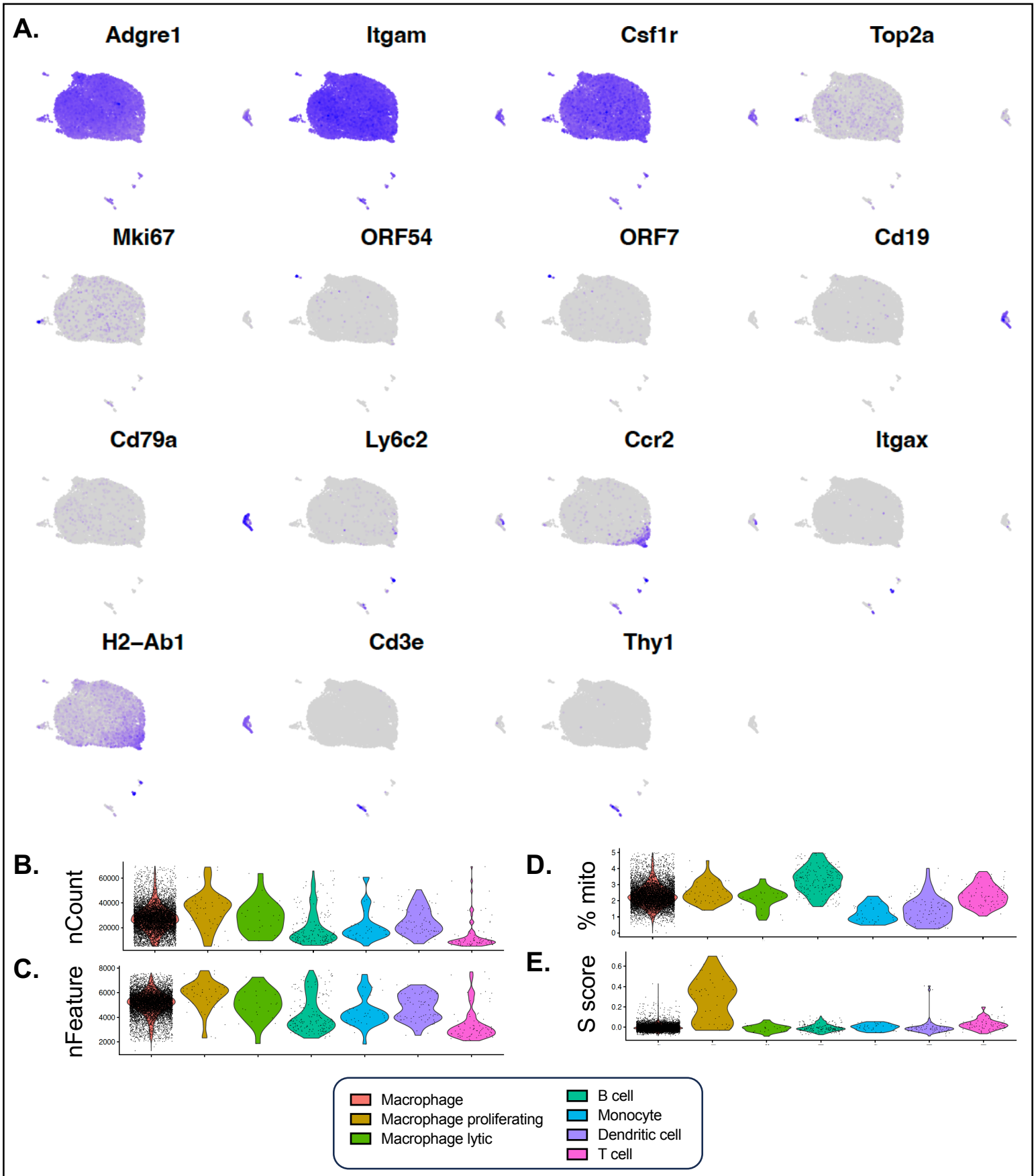

Vragel et al
Fig. S1

Supplemental Figure 1 (Figure S1). Single cell RNA sequencing analysis of acute MHV68 macrophage infection. Data correspond to **Figure 1**. (A) Visualization of gene expression based on UMAP topography in Fig. 1A. Maximal expression is designated by purple, with absence of detection designated by gray. Each panel depicts a distinct lineage-defining gene used to identify cell types in Fig. 1, with signature genes for each cell type as follows. Macrophage: Adgre1 (encodes the F4/80 protein), Itgam (encodes the CD11b protein). Macrophage proliferative: Top2a, Mki67. Macrophage lytic: ORF54, ORF7. B cell: Cd19, CD79a. Monocyte: Ly6c2, Ccr2. Dendritic cell: Itgax, H2-Ab1. T cell: Cd3d, Thy1. (B-E) scRNA-seq quality control metrics across cell subsets, including (B) UMI Count, (C) Features, (D) % mitochondrial reads, and (E) S score, a proliferation-associated gene signature.

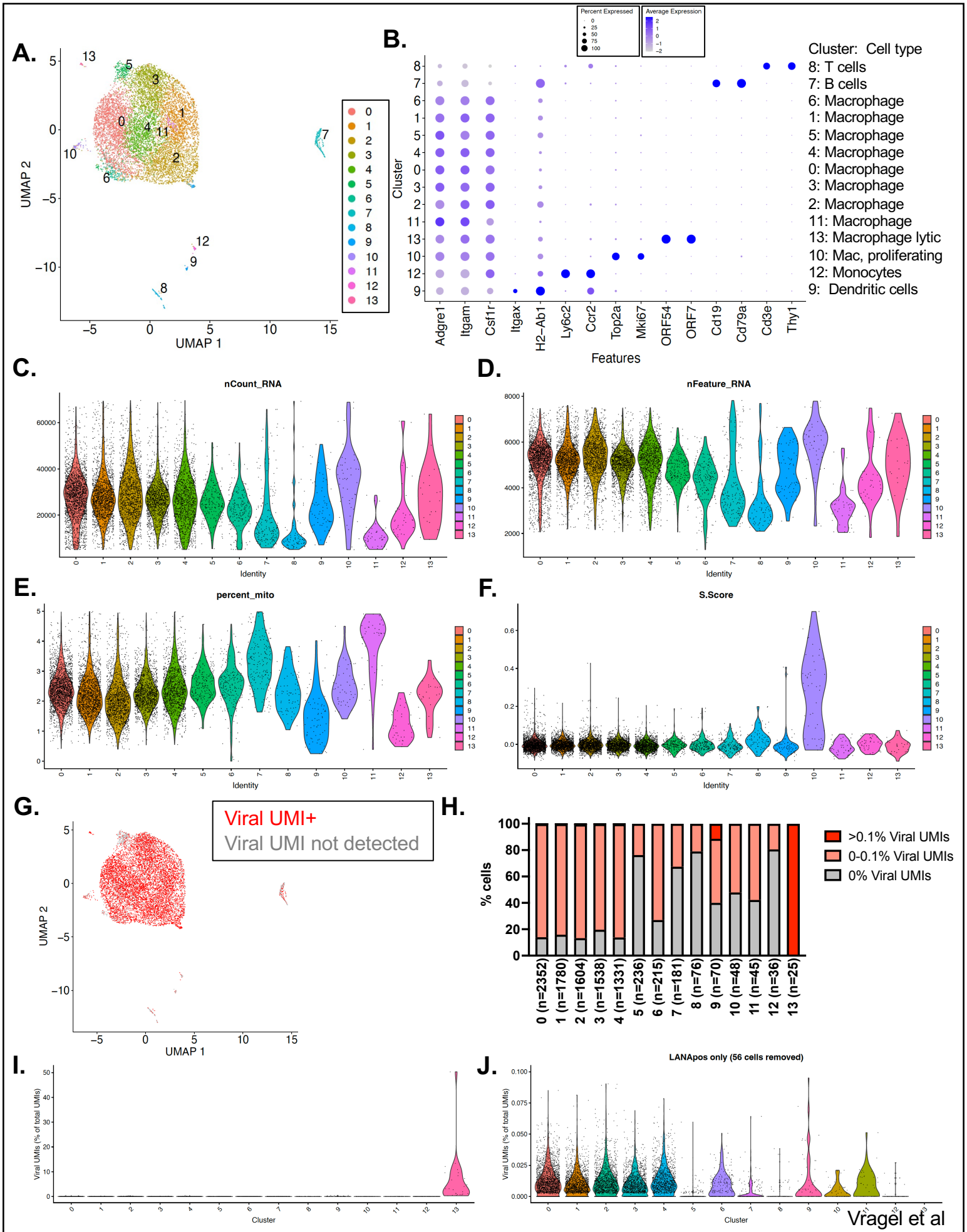

Vragel et al
Fig. S2

Figure S2. Single cell RNA sequencing analysis of acute MHV68 macrophage infection analyzed using a higher number of cell clusters. Data correspond to **Figure 1**, with scRNA-seq subjected to Seurat-based designation of 14 clusters. **(A)** UMAP visualization of Seurat-defined clusters. **(B)** Visualization of the frequency and magnitude of host gene expression across clusters, with cell type designation indicated on right. **(C-F)** Quality control metrics across the 14 clusters, including (C) UMI Count, (D) Features, (E) % mitochondrial reads, and (F) S score, a proliferation-associated gene signature. **(G)** UMAP visualization of cells with at least 1 detectable viral UMI per cell identified in red. **(H)** Frequency of cell subsets stratified by the frequency of viral UMIs of total UMIs detected per cell. **(I-J)** Percentage of viral UMIs out of total UMIs across clusters (panel I, y axis range from 0-50%), or (J) focused only on the majority of virus positive cells (y axis range, 0-0.1%; excluding 56 cells with % viral UMI > 0.1). Data are from 9,537 cells, with clusters containing between 25-2,532 cells. Panel G is included to provide a frame of reference and depicts the same data as in Figure 1D.

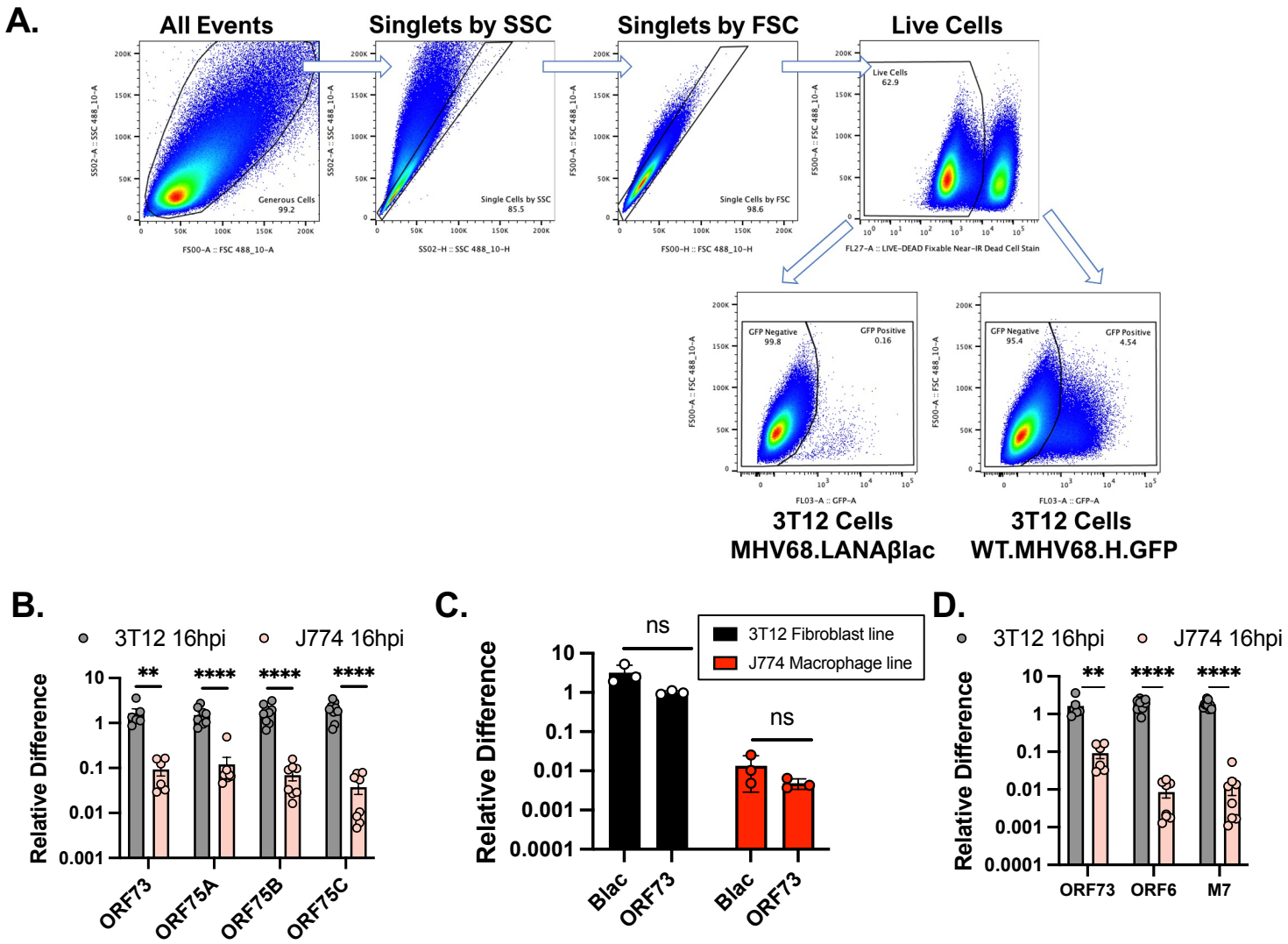

Vragel et al
Fig. S3

Figure S3. Flow cytometry gating strategy and viral gene expression during MHV68 infection. (A) Flow cytometry gating strategy to analyze MHV68-infected cells, in support of **Figure 3E**. 3T12 cells infected with MHV68 LANAblac or WT.MHV68.H.GFP were analyzed by flow cytometry, using sequential focused analysis (i.e. ”gating”) to consider cells that are single cells (defined sequentially as “Singlets by SSC” and “Singlets by FSC”) that are viable (”Live cells”) defined by exclusion of a dye that identifies dead cells. Live cells were then analyzed for GFP fluorescence as measured by the GFP detection channel. Cells infected with MHV68.LANAβlac, without additional of the CCF2 fluorescent substrate, identified background fluorescence, in contrast to samples infected with MHV68.H.GFP which encoded GFP. Controls included single-stained samples with only one stain to define the bounds of a gate for the fluorophore of interest. **(B-D)** Viral gene expression defined by qRT-PCR in 3T12 or J774 cells infected with WT MHV68.LANAblac (MOI=1) at 16 hpi (B,D) or 24 hpi (C) in support of **Figure 3F-G**. Data show mean ± SEM from 3 independent experiments with 3 biological replicates measured in technical triplicates per experiment (depicted by individual symbols) (B,D) or from 1 experiment with 3 biological replicates measured in technical triplicates, with ORF73 data from Fig. 2B (C). Statistical analysis was done using unpaired t test with statistically significant differences as indicated. ** $p<0.01$, ***$p<0.001$, ****$p<0.0001$. ns, no statistical significance detected.

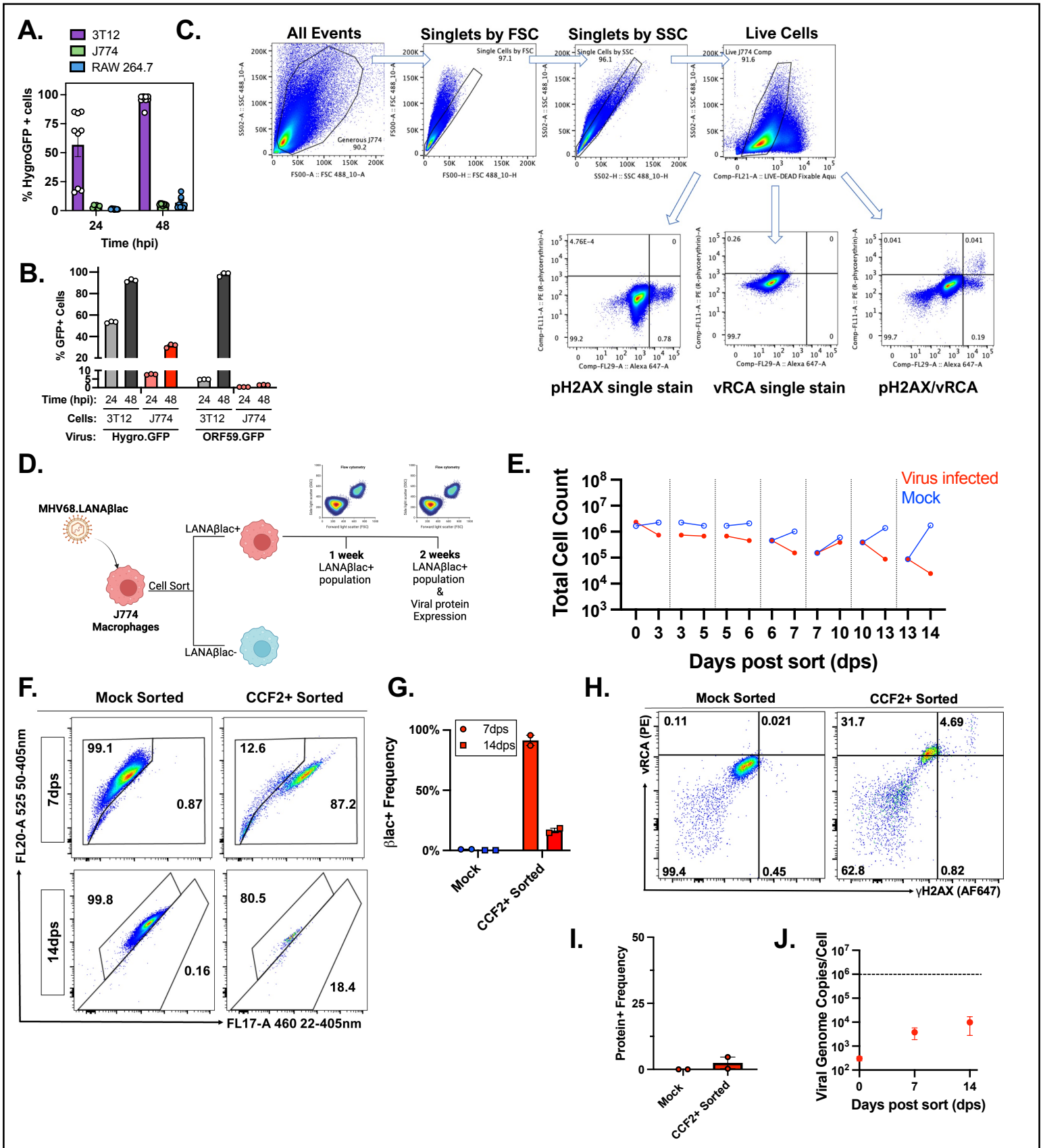

Vragel et al
Fig. S4

Figure S4. Gating of flow cytometry analysis of MHV68 LANAβlac infected J774 cells for lytic protein markers. (A) Analysis of GFP expression in 3T12 fibroblasts, J774 and RAW264.7 macrophage cell lines at 24 or 48 hpi, following infection with MHV68.H.GFP (MOI=1). **(B)** Gating strategy to analyze vRCA and γH2AX expression in MHV68-infected J774 cells, in support of **Figure 4C**. Cells were analyzed by flow cytometry, using sequential focused analysis (i.e. ”gating”) to consider cells that are single cells (defined sequentially as “Singlets by SSC” and “Singlets by FSC”) that are viable (”Live cells”) defined by exclusion of a dye that identifies dead cells. Live cells were then analyzed for antibody binding for lytic protein markers. Gate boundaries were defined using a combination of “single stain” samples, containing only the fluorophore of interest, and “full minus one” controls, lacking the antibody in the fluorescent channel of the excluded fluorophore (not shown). **(C-I)** Analysis of MHV68-infected, FACS-purified J774 cells over time. **(C)** Experimental overview with J774 macrophages infected with MHV68.LANAβlac (MOI=1), followed by sorting for LANAblac+ cells defined based on CCF2 substrate cleavage. Mock and LANAblac+ sorted cells were cultured and analyzed over 14 days. **(D)** Total cell counts over the course of the study, with each vertical line indicate a subsequent cell passage. **(E)** Flow cytometric analysis of LANAβlac expression defined by cleavage of the CCF2 fluorescent beta-lactamase substrate, analyzing single, viable cells, with values in the right gate defining the frequency of cells with CCF2 substrate cleavage. **(F)** Quantification of LANAβlac+ cell frequency defined by flow cytometry, as in panel E. **(G)** Flow cytometric analysis of MHV68 lytic cycle-associated proteins (vRCA, γH2AX) at 14 dps, comparing mock (left) or CCF2-sorted, LANAblac+ cells (right). Data depict events that were single, viable cells, with values defining the frequency of cells with vRCA and/or phosphorylated host γH2AX, indicative of lytic MHV68 infection, as in panel B. **(H)** Frequency of vRCA+ γH2AX+ cells defined by flow cytometry, as in panel G. **(I)** Quantitation of viral DNA by qPCR. Dotted line indicates mean 3T12 viral genome copies/cell at 72 hpi. Data show mean ± SEM from 3 independent experiments with 3 biological replicates per experiment (depicted by individual symbols) (A) or from 2 independent experiments.